NAVAL POSTGRADUATE SCHOOL
Monterey, California

THESIS

A NUMERICAL STUDY OF EDDY STEERING BY BACKGROUND FLOWS

by

Ray T. Huddleston, Jr.

December 1990

Thesis Advisor D. C. Smith, IV

Unclassified

ecurity classification of this page

REPORT DOCUMENTATION PAGE

1a Report Security Classification Unclassified		1b Restrictive Markings	
2a Security Classification Authority		3 Distribution/Availability of Report	
2b Declassification/Downgrading Schedule		Approved for public release; distribution is unlimited.	
4 Performing Organization Report Number(s)		5 Monitoring Organization Report Number(s)	
6a Name of Performing Organization Naval Postgraduate School	6b Office Symbol *(if applicable)* 35	7a Name of Monitoring Organization Naval Postgraduate School	
6c Address *(city, state, and ZIP code)* Monterey, CA 93943-5000		7b Address *(city, state, and ZIP code)* Monterey, CA 93943-5000	
8a Name of Funding/Sponsoring Organization	8b Office Symbol *(if applicable)*	9 Procurement Instrument Identification Number	
8c Address *(city, state, and ZIP code)*		10 Source of Funding Numbers	
		Program Element No / Project No / Task No / Work Unit Accession No	

11 Title *(include security classification)* A NUMERICAL STUDY OF EDDY STEERING BY BACKGROUND FLOWS

12 Personal Author(s) Ray T. Huddleston, Jr.

13a Type of Report	13b Time Covered	14 Date of Report *(year, month, day)*	15 Page Count
Master's Thesis	From To	December 1990	64

16 Supplementary Notation The views expressed in this thesis are those of the author and do not reflect the official policy or position of the Department of Defense or the U.S. Government.

17 Cosati Codes			18 Subject Terms *(continue on reverse if necessary and identify by block number)*
Field	Group	Subgroup	Oceanography, eddy steering by background flows.

19 Abstract *(continue on reverse if necessary and identify by block number)*

Gulf Stream warm core rings are intense, isolated eddies which form to the north of the Gulf Stream from cutoff meanders which detach from the Stream. After their formation they are embedded in the cooler Slope Water which flows generally westward, impinging on the continental slope near 70° W. Observations indicate that the Slope Water flows westward at approximately 5 cm/s. In this study, the effect of background shear flows on anticyclonic eddy motion is examined using a two layer primitive equation model. The effect of various lateral shear profiles is considered for barotropic and equivalent barotropic eddies. Results indicate that eddy zonal propagation is dependent on the eddy initial vertical profile and form of the background shear lateral profile. Eddy meridional speeds are found to be insensitive to background shear profile or strength.

20 Distribution/Availability of Abstract	21 Abstract Security Classification	
☒ unclassified/unlimited ☐ same as report ☐ DTIC users	Unclassified	
22a Name of Responsible Individual D. C. Smith, IV	22b Telephone *(include Area code)* (408) 646-3350	22c Office Symbol OC/Si

OD FORM 1473,84 MAR

83 APR edition may be used until exhausted
All other editions are obsolete

security classification of this page

Unclassified

Approved for public release; distribution is unlimited.

A Numerical Study of Eddy Steering by Background Flows

by

Ray T. Huddleston, Jr.
Lieutenant, National Oceanic and Atmospheric Administration
B.S., University of Texas at Austin, 1983

Submitted in partial fulfillment of the
requirements for the degree of

MASTER OF SCIENCE IN METEOROLOGY AND PHYSICAL OCEANOGRAPHY

from the

NAVAL POSTGRADUATE SCHOOL
December 1990

ABSTRACT

Gulf Stream warm core rings are intense, isolated eddies which form to the north of the Gulf Stream from cutoff meanders which detach from the Stream. After their formation they are embedded in the cooler Slope Water which flows generally westward, impinging on the continental slope near 70° W. Observations indicate that the Slope Water flows westward at approximately 5 cm/s. In this study, the effect of background shear flows on anticyclonic eddy motion is examined using a two layer primitive equation model. The effect of various lateral shear profiles is considered for barotropic and equivalent barotropic eddies. Results indicate that eddy zonal propagation is dependent on the eddy initial vertical profile and form of the background shear lateral profile. Eddy meridional speeds are found to be insensitive to background shear profile or strength.

TABLE OF CONTENTS

LIST OF TABLES

LIST OF FIGURES

ACKNOWLEDGEMENTS

I express my gratitude to Professor David C. Smith, IV for his advice and guidance during the writing of this work. I thank Arlene Bird for her expertise in programming.

To Barbara, without whose support I would never have gotten this far in life, a special thanks.

I. INTRODUCTION

The motion of western boundary current eddies, such as Gulf Stream rings, has been the subject of numerous observational and theoretical studies. These studies have illustrated that rings move westward due to planetary rotation, have meridional motions associated with azimuthal distortions, and are advected by background flows.

The westward drift of an eddy due to planetary rotation or the β-effect was discussed by Rossby (1948). An eddy can be viewed as a summation of Rossby waves. It decays due to Rossby wave dispersion. Long Rossby waves travel faster to the west than short waves, leading to a spreading of energy away from the eddy. Dispersion also produces an azimuthal distortion of the eddy which introduces a secondary propagation mechanism which is northward for cyclones and southward for anticyclones. This was illustrated in a series expansion by Adem (1956). This distortion was further examined in numerical experiments of isolated eddies by McWilliams and Flierl (1979), and Mied and Lindemann (1979). The effect of asymmetry on a β-plane eddy can be seen by separating the eddy into symmetric and asymmetric parts. Smith and Bird (1989) show this decomposition, which illustrates that the asymmetric part is dipolar and advects the eddy north or south depending on the sense of rotation. These previous studies then suggest that anticyclones in a quiescent background should move southwestward. Eddies embedded in a broader background flow may also have a component of propagation associated with mean flow advection.

Cornillon *et al.* (1989) have estimated the rate of translation of anticyclonic warm core rings in the Slope Water north of the Gulf Stream (Figure 1 on page 2). Their estimates are based on satellite images and provide ring translation rate relative to the surrounding Slope Water. They focus on rings which are to the east of 70° W. Rings and the Slope Water east of 70° W are not topographically steered by the continental slope as they flow to the west. Cornillon *et al.* (1989) also restrict their analysis to rings which are not interacting with the Gulf Stream. Their results, based on 11 rings, indicate a northward component (Figure 2 on page 3) of ring propagation relative to the Slope Water. This northward component is at odds with theoretical considerations which suggest that anticyclones should have a southward component of propagation.

In another study of warm core ring translation, Auer (1987) documents the motion of 66 warm core rings. His study is not limited to eddies away from the Gulf Stream or

Figure 1. Gulf Stream Axis Topology: White line indicates mean Gulf Stream axis. Black lines indicate actual axis locations. (Courtesy of P. Cornillon)

topography. Figure 3 on page 4 shows observations of warm core ring paths in his study. This figure indicates a generally southwestward warm core ring path.

The effect of background flow on eddy motion has been studied by Matsuura and Yamagata (1982). Their study considers eddies which are larger than the Rossby radius

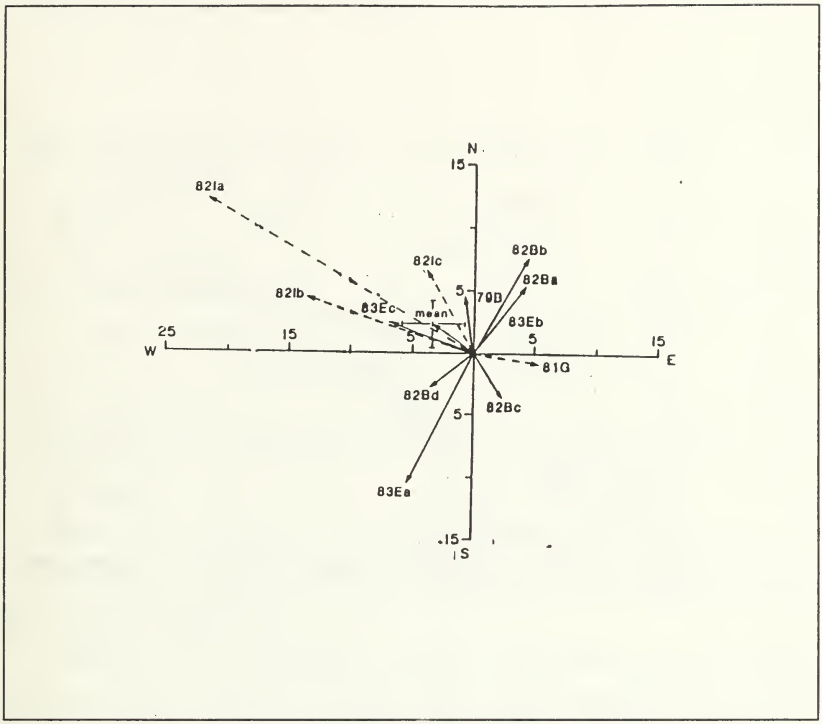

Figure 2. Warm Core Ring Translation Vectors (Cornillon *et al.*,1989): Velocity (cm/s) of warm core rings relative to the Slope Water based on depth averaged Slope Water velocity. Solid vectors for velocities west of the New England Seamounts. Dashed vectors for velocities east of the seamounts.

of deformation. For eddies of this size, planetary dispersion is weak and can be considered a second order effect. They consider background zonal geostrophic flow fields which have a corresponding meridional sea surface tilt. The surface tilt represents a meridional background vorticity gradient and hence introduces an additional source of dispersion. They then show that the weak dispersion associated with the sea surface tilt can exactly cancel the weak dispersion associated with the planetary β-effect. For this reason, eddies in their numerical simulations with a uniform background flow do not disperse, but propagate as symmetric features. The applicability of this result to warm

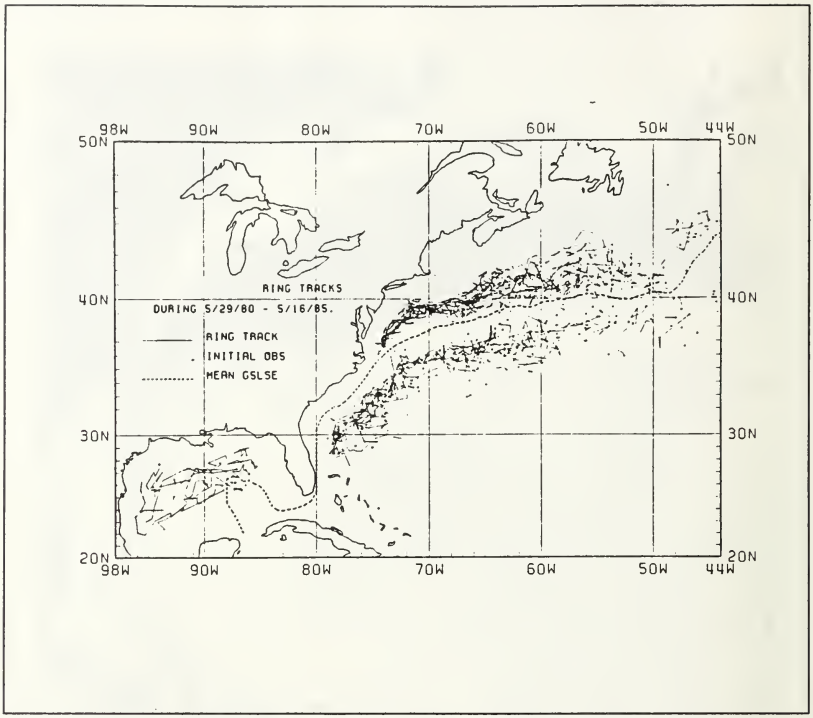

Figure 3. Warm Core Ring Translation (Auer,1987): Observed warm core and cold core ring tracks for 5 years. The dashed line is the 5-year mean Gulf Stream Landward Surface Edge (GSLSE).

core ring propagation is questionable because of the assumption of a large eddy size. Warm Core rings have a radius (75 km) comparable to the Rossby radius of deformation.

The interaction of rings with horizontal and vertical shear was studied by Nof and Shi (1989) using a two-layer model based on f-plane quasigeostrophic equations. To obtain analytic solutions they assumed that the background shear was weak compared to the ring's shear. They found that eccentricity in rings can result in response to horizontal shear in the lower layer but that the rings remain circular in response to horizontal shear in the upper layer. Nof and Shi's results, applied to warm core rings,

suggest that the major axis of the elliptical ring would be aligned with the background flow if the background flow had anticyclonic shear in the lower layer. If the flow in the lower layer was cyclonically-sheared, the major axis would be perpendicular to the flow direction. Their study concentrates on eddy shape and not on eddy propagation and hence does not appear to explain the northward component of motion for warm core rings in the Slope water reported by Cornillon *et al.* (1989).

In a study of the Great Red Spot on Jupiter, Ingersoll and Cuong (1981) examined the stability of isolated vortices in a two layer lateral shear flow. In their study, an upper layer vortex of size greater than the internal Rossby radius of deformation was embedded in a meridional lateral shear $\bar{u}(y)$ which is the same in both layers outside of the vortex. They chose a $\bar{u}(y)$ profile which was barotropically stable. An important quantity in their results is the ratio of potential to kinetic energy in the vortex. For values of this ratio exceeding 5.0, the vortex is unstable and is rapidly sheared apart by the basic flow. For $\frac{PE}{KE}$ values of approximately 1 the vortices are stable. In our study and in Gulf Stream rings, this value is also O(1). None of the solutions shown here exhibit these instabilities.

These various studies indicate the effect of background shear on eddy shape, eddy stability, eddy decay and eddy motion. The purpose of this study is to determine the effects of background shear on eddy motion with emphasis on Gulf Stream warm core ring motion in the Slope Water.

This paper is organized as follows. The model is described in Chapter III, with experiment numerical parameters. Numerical results obtained for initially barotropic and initially equivalent barotropic experiments are presented in Chapter III. Analysis of model results is contained in Chapters IV, V, and VI, followed by discussion and conclusions.

II. NUMERICAL MODEL

A. TECHNIQUE AND MODEL PARAMETERS

Experiments are performed using a two-layer primitive equation semi-implicit numerical scheme. Motion in each layer is governed by a momentum equation:

$$\frac{\partial V_i}{\partial t} + (\nabla \cdot V_i + V_i \cdot \nabla)v_i + \hat{k} \times fV_i = - h_i \nabla P_i - B_h \nabla^4 V_i \qquad [1]$$

and a continuity equation:

$$\frac{\partial h_i}{\partial t} + \nabla \cdot V_i = 0 \qquad [2]$$

for layer (i = 1 upper and i = 2 lower) thickness h_i, transports V_i , and velocities v_i. The hydrostatic and Boussinesq approximations have been made. Density is constant in each layer. No mixing is allowed across the interface. Thermodynamic processes are not considered. Subgrid scale dissipation processes are represented by a biharmonic operator on transport. All notation is defined in Appendix A.

The numerical scheme (Figure 4 on page 8) has been used in numerous ocean mesoscale circulation studies (Hurlburt and Thompson (1980); Smith and O'Brien (1983)) where it is more fully discussed. It has been shown to conserve energy in the absence of dissipation. The model has been compared with analytic solutions for linear eddies (as discussed in Smith and Reid, 1982). The correct representation of Rossby wave dispersion processes in the model was verified.

B. BOUNDARY AND INITIAL CONDITIONS

A rectangular (1100 x 800 km) finite difference gridded domain is used. Grid resolution ($2\Delta x$) is 20 km. The initial state consists of a Gaussian eddy:

$$h(x,y) = A \exp\left(- \frac{x^2 + y^2}{2L_e^2} \right) \qquad [3]$$

in gradient balance in mid-basin. L_e is the e-folding width scale for eddy. The amplitude of the Gaussian distribution was chosen to give a maximum velocity (v_{max}) of approximately 1 m/s in all experiments. Experiments are initialized with either barotropic or upper layer (equivalent barotropic) eddy velocity distributions. The background shear

is initially barotropic in all cases. Upper layer mean thickness is chosen to be 1000 m. The lower layer mean thickness is 4000 m. The first internal Rossby radius of deformation (R_d) associated with this layer thickness distribution is approximately 40 km. No variable bottom topography is considered.

A radiation condition was used on the downstream (right) boundary in all model simulations. The radiation condition (Camerlengo and O'Brien,1980) advects flow out of the basin (at speed $\frac{\Delta x}{\Delta t}$) when flow is outward adjacent to the boundary. The north and south boundaries are no-slip walls where both tangential and normal flow velocities are set equal to zero.

Table 1 on page 10 provides initial conditions for the experiments. All simulations were integrated for a duration of 45 days. Variable parameters in the study are eddy vertical structure and the structure of the background shear. The biharmonic friction coefficient, B_h, is $.2x10^{11}$. This value efficiently damps grid scale noise, leaving the eddy scales relatively undamped.

The background shear flow is defined in several ways. Initial experiments (Chapter III C,D) have a mean flow which is barotropic ($u_1 = u_2$) with a linear surface tilt from north to south:

$$h(y) = .4\frac{y}{L} \qquad [4]$$

where L is the domain length in the meridional direction and y is the distance from the southern boundary. This height field distribution has a uniform westward flow with no lateral shear. The flow velocity can be estimated from geostrophy:

$$u = \frac{-g}{f}\frac{\partial h}{\partial y} = \frac{(10m/(s^2))(.4m)}{(10^{-4}s^{-1})(780km)} = .05m/s \qquad [5]$$

This velocity is consistent with that observed by Cornillon *et al.* (1989) for the warm core ring region.

The second set of experiments (Chapter III E,F) involves a lateral shear in the mean flow:

$$h(y) = \frac{1.6}{2}(1 - \frac{y}{L})^2 \qquad [6]$$

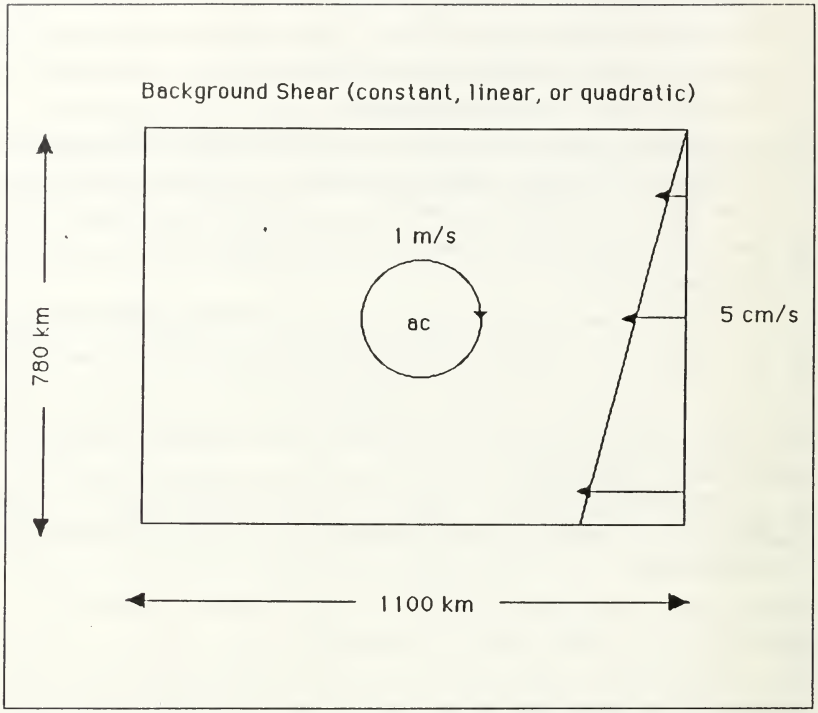

Figure 4. Model Domain for Numerical Study: Linear shear is illustrated but constant and quadratic shear cases are also considered.

$$u = \frac{-g}{f}\frac{\partial h}{\partial y} = -\frac{g}{f}\,1.6(1-\frac{y}{L})(\frac{-1}{L}) = \frac{1.6g}{fL} - \frac{1.6gy}{fL^2} \qquad [7]$$

The velocity shear is linear in this case with velocity equal to 5 cm/s at mid basin. As is discussed below, this shear profile has anticyclonic relative vorticity, but provides no β-effect ($\frac{\partial \zeta}{\partial y}$) for the eddy. The lateral profile of the zonal flow is shown in Figure 5 on page 9 for this case and the other shear profiles.

The final experiments (Chapter III G,H) have a parabolic height field:

$$h(y) = \frac{1.6}{3}(1-\frac{y}{L})^3 \qquad [8]$$

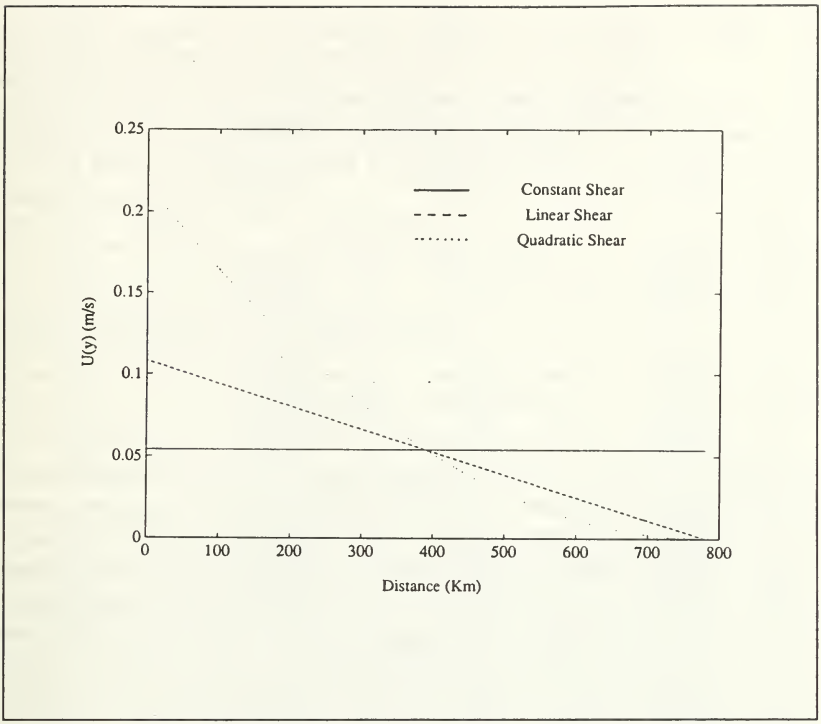

Figure 5. Velocity Profiles for Different Shear Cases: The velocity profiles for the constant shear, linear shear, and quadratic shear case.

$$u = \frac{-g}{f}\frac{\partial h}{\partial y} = -\frac{g}{f}3(1-\frac{y}{L})^2(\frac{-1}{L}) \qquad [9]$$

For a parabolic surface distribution, the velocity distribution is quadratic. This lateral profile also has anticyclonic shear flow. In each of the sets of experiments the flow is initially barotropic ($u_1 = u_2$) and equal to approximately 5 cm/s at mid-domain. This choice of velocity at mid-domain is based on the observations of Cornillon *et al.* (1989).

1. Preliminary considerations

The characteristics of the lateral shear profiles chosen above can be examined to determine possible β-effects on the eddy. In the first experiments a uniform back-

Table 1. **EXPERIMENT INITIAL PARAMETERS:** Experiment names are defined by a four character code. The first two indicates barotropic (BT) or baroclinic (BC), the third character indicates the flow pattern (No shear, Constant, Linear, or Quadratic shear) and the last character indicates mid basin flow (W for .05 m/s and S for .108 m/s).

Experiments	Mean Flow Velocity at Mid Basin (m/s)	Initial Eddy Vertical Structure	Initial Eddy Velocity $\frac{u_1}{u_2}$ (m/s)
No Mean Flow			
BTNS	0	Barotropic	1/1
BCNS	0	Baroclinic	1/0
Constant Flow			
BTCW	.05	Barotropic	1/1
BTCS	.108	Barotropic	1/1
BCCW	.05	Baroclinic	1/0
BCCS	.108	Baroclinic	1/0
Linear Flow			
BTLW	.05	Barotropic	1/1
BTLS	.108	Barotropic	1/1
BCLW	.05	Baroclinic	1/0
BCLS	.108	Baroclinic	1/0
Quadratic Flow			
BTQW	.05	Barotropic	1/1
BTQS	.108	Barotropic	1/1
BCQW	.05	Baroclinic	1/0
BCQS	.108	Baroclinic	1/0

ground flow is present with no lateral shear. In the second set of experiments the surface tilt is quadratic. In the third set of experiments the surface is parabolic. Relative vorticity is defined:

$$\zeta = \frac{\partial v}{\partial x} - \frac{\partial u}{\partial y} = -\frac{\partial u}{\partial y} \qquad [10]$$

as no mean flow in the meridional direction is defined. Relative vorticity is equal to zero for the first set (constant flow) of experiments. For the second set (linear shear) relative vorticity is:

$$\zeta = -\frac{2g}{fL^2} \qquad [11]$$

The north-south variation of relative vorticity or a β-effect for the eddy, provided by the background flow, is zero in this case.

In the third set experiments, the surface tilt is parabolic. The relative vorticity in this case is not a constant.

$$\zeta = -\frac{\partial u}{\partial y} = \frac{3.2g}{fL^2} - \frac{3.2gy}{fL^3} \qquad [12]$$

The associated vorticity gradient is:

$$\frac{\partial \zeta}{\partial y} = \frac{3.2g}{fL^3} = -7.1x10^{-13} m^{-1} s^{-1} \qquad [13]$$

This β-effect is associated with the background shear in the third set of experiments. This may augment or offset the planetary β-effect. If this were to occur, the dispersive decay of the eddy due to planetary β would be altered. This would change the eddy decay rate and direction of propagation. This was found to be the case in the results of Matsuura and Yamagata (1982) where the planetary dispersive decay of an eddy was exactly cancelled by the β-effect associated with the shear flow. In that case the meridional motion of the vortex did not occur and the motion was largely zonal. In our case however, the shear-related β-effect is one order of magnitude smaller than the planetary β-effect. The nondispersive behavior of eddies as seen by Matsuura and Yamagata (1982) is not anticipated in these experiments.

III. MODEL RESULTS

A. BAROTROPIC EDDY, NO SHEAR

For comparison with subsequent experiments with background shear, a barotropic experiment with no mean flow (BTNS) is shown in Figure 6 on page 13. This experiment illustrates the behavior of an anticyclone as influenced by planetary and nonlinear self advection. As in previous isolated eddy studies, the eddy decays by Rossby wave radiation which spins up adjacent eddies. Long Rossby waves travel faster to west than do the short waves causing a distortion in the eddy. The net effect of the dispersion is to broaden the frontal zone in the leading edge of the eddy and to steepen the trailing edge. In barotropic simulations, the layers evolve in phase and the flow remains largely barotropic. This can be seen by comparing upper and lower layer relative vorticity, Figure 6 on page 13. This distribution can be described by an azimuthal mode one correction to a circular shape. While westward motion initially occurs due to β, the azimuthal mode distribution leads to a southward component of propagation. By decomposing the eddy into an axisymmetric and nonsymmetric part and removing the axisymmetric part (Figure 7 on page 14), it can be seen that the nonsymmetric part associated with azimuthal mode one is dipolar. The dipolar part then advects the symmetric part southward. In this experiment the mean eddy speed is .17 km/day to the west and 4.57 km/day to the south. The eddy speeds for this and subsequent experiments are shown in Appendix B. The trajectory for the eddy center for this case and subsequent barotropic cases are shown in Figure 8 on page 15.

Previous experiments with barotropic eddies in two layer models (McWilliams and Flierl (1979); Mied and Lindemann (1979)) have shown that barotropic eddies decay barotropically with very little energy transfer into the baroclinic mode. Barotropic eddies also disperse faster than baroclinic eddies. This provides greater azimuthal mode one distortion and hence greater southward propagation.

B. BAROCLINIC EDDY, NO SHEAR

A baroclinic eddy experiment with no mean flow (BCNS, Figure 9 on page 16) illustrates these differences between barotropic and baroclinic eddies. This figure shows that the degree of dispersion is less. That baroclinic eddies are less dispersive can be seen

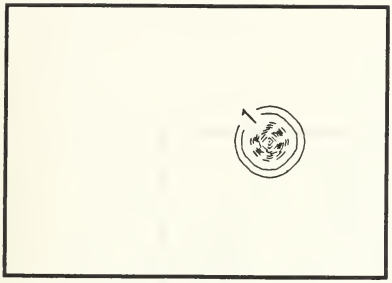

Day 0 Upper Layer Relative Vorticity

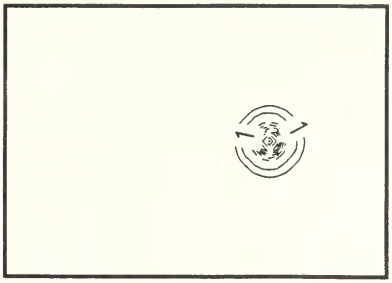

Day 0 Lower Layer Relative Vorticity

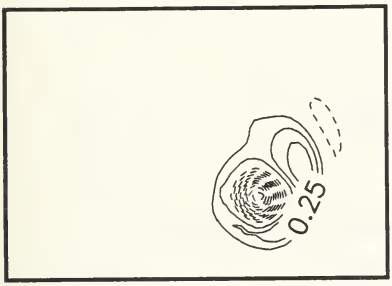

Day 22 Upper Layer Relative Vorticity

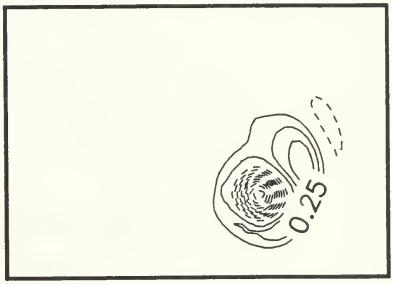

Day 22 Lower Layer Relative Vorticity

Day 37 Upper Layer Relative Vorticity

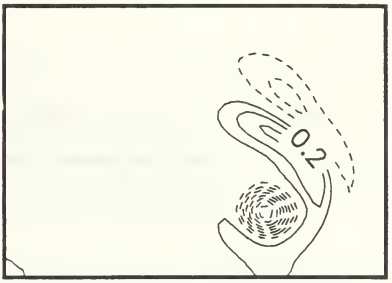

Day 37 Lower Layer Relative Vorticity

Figure 6. Barotropic Eddy, No Shear: The panels are contours of relative vorticity at days 0, 22, and 37. Positive values are solid, negative values are dashed, and values are $10^{-5}s^{-1}$. The contour intervals equal .5x $10^{-5}s^{-1}$ (day 0), .125x$10^{-5}s^{-1}$ (day 22), and .1x$10^{-5}s^{-1}$ (day 37). North is at the top of the figure.

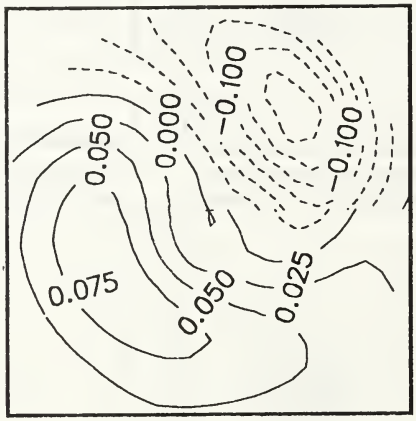

Figure 7. Eddy in Axisymmetric and Nonsymmetric Components (day 22): Barotropic eddy no shear, day 22 with axisymmetric component removed illustrating azimuthal mode one structure. The contour is surface height anomaly after the height associated with the axisymmetric signature of the eddy has been removed. The contour interval is .025x 10^{-1}m.

by considering the characteristics of Rossby waves. The Rossby wave dispersion relation is written:

$$\omega = \frac{-\beta k}{k^2 + l^2 + \frac{1}{R_d^2}} \qquad [14]$$

where k and l are wavenumbers in x, y direction and R_d is Rossby radius of deformation.

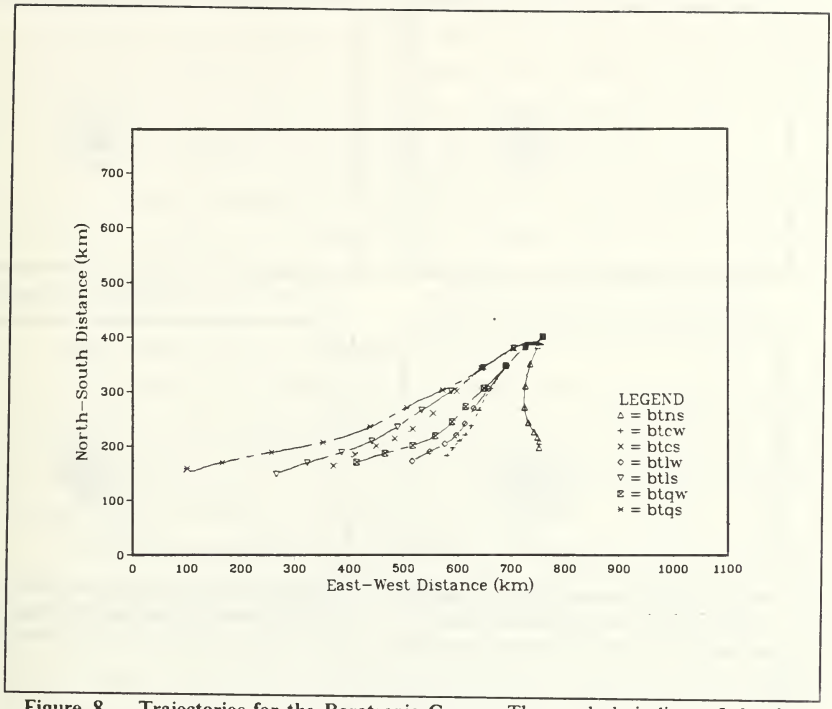

Figure 8. Trajectories for the Barotropic Cases: The symbols indicate 5 day intervals.

For barotropic eddies the term involving the Rossby radius involves the external Rossby radius and is negligible compared to k and l. This makes all the barotropic waves dispersive. For baroclinic eddies the internal Rossby radius is more comparable to the eddy scale and is not negligible. This makes a portion of the waves nondispersive. Associated with the less dispersive nature of the baroclinic eddy is less azimuthal mode one distortion and a smaller southward component. Westward and southward eddy speeds are 1.5 and 3.4 km/day respectively. The trajectory for the eddy center for this case and subsequent baroclinic cases are shown in Figure 10 on page 18 and Figure 11 on page 19. Lower layer relative vorticity (Figure 9 on page 16) illustrates that lower layer circulations are the result of vortex stretching of quiescent lower layer fluid by the moving

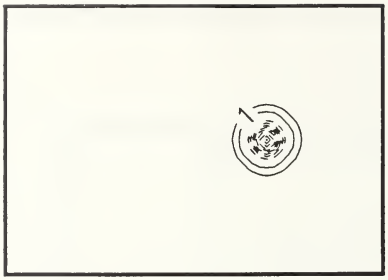

Day 0 Upper Layer Relative Vorticity

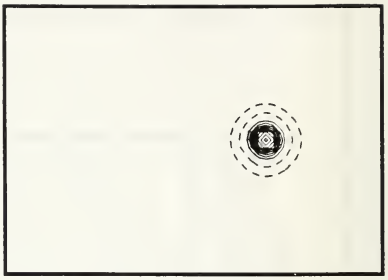

Day 0 Lower Layer Relative Vorticity

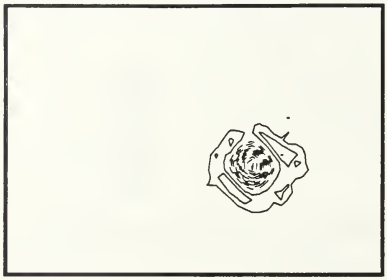

Day 22 Upper Layer Relative Vorticity

Day 22 Lower Layer Relative Vorticity

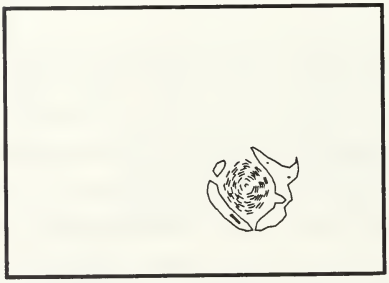

Day 37 Upper Layer Relative Vorticity

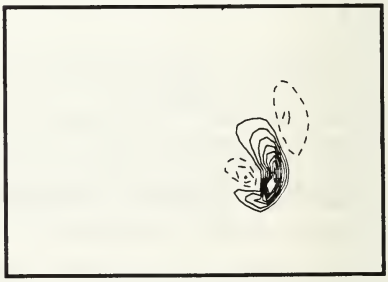

Day 37 Lower Layer Relative Vorticity

Figure 9. Baroclinic Eddy, No Shear: The panels are contours of relative vorticity at days 0, 22, and 37. Positive values are solid, negative values are dashed, and values are $10^{-5}s^{-1}$. The contour intervals equal .5x $10^{-5}s^{-1}$ (day 0), .125x$10^{-5}s^{-1}$ (day 22), and .1x$10^{-5}s^{-1}$ (day 37). North is at the top of the figure.

upper layer eddy. As argued by Cushman-Roisin *et al.* (1989), fluid columns to the west of the eddy are vortex squashed as the anticyclone goes over them. Fluid columns initially under the anticyclone are vortex stretched as the anticyclone moves westward. Cushman-Roisin *et al.* (1989) argue that these secondary circulations combine to advect the upper layer anticyclone to the south (see Figure 12 on page 20).

A comparison with the reduced gravity results of Smith and Reid (1982) where upper layer eddies over a motionless lower layer are considered indicates that this lower layer effect does contribute to the southward motion. In Smith and Reid (1982) a comparable size and strength eddy moved in the meridional direction at 1 km/day in contrast to 3.4 km/day in BCNS.

C. BAROTROPIC EDDY, CONSTANT SHEAR

For comparison with the lateral shear flow cases below, several experiments with constant .05 m/s background flow are discussed. Figure 13 on page 21 shows relative vorticity for barotropic case BTCW. As in case BTNS, rapid barotropic dispersion gives rise to a trailing cyclonic vortex to the northeast of the anticyclone. The anticyclone moves south (4.89 km/day) and west (4.02 km/day).

The meridional propagation speed of the eddy is comparable to no mean flow case BTNS. The zonal speed is substantially higher than in BTNS. The eddy speed to the west (4.02 km/day) is 10% less than the mean flow speed (5 cm/s) (5 cm/s equals 4.32 km/day) plus zonal eddy speed in the no shear case BTNS (.17 km/day) suggesting that the two effects on eddy motion are not simply additive. Appendix B shows the zonal and meridional speeds for this and other barotropic cases.

The surface height anomaly fields for this experiment show that a divergent region appears to the west of the eddy. The eddy thus has a substantial effect on the background flow upstream and downstream of the eddy. As in experiment BTNS, the layers evolve in phase with no significant transfer of energy into the baroclinic component.

D. BAROCLINIC EDDY, CONSTANT SHEAR

Figure 14 on page 22 shows the evolution of corresponding baroclinic case BCCW for constant background flow (.05 m/s). As with no mean flow (baroclinic case BCNS), the eddy is less dispersive than the preceding barotropic case. A weak trailing cyclone appears to the east of the upper layer anticyclone in relative vorticity. This cyclone is also evident as a northward distortion in the mean flow lines to the east of the anticyclone in the surface height anomaly. This plot also shows that while an upstream effect on the mean flow is caused by the eddy, no downstream effect (as in BTCS) is

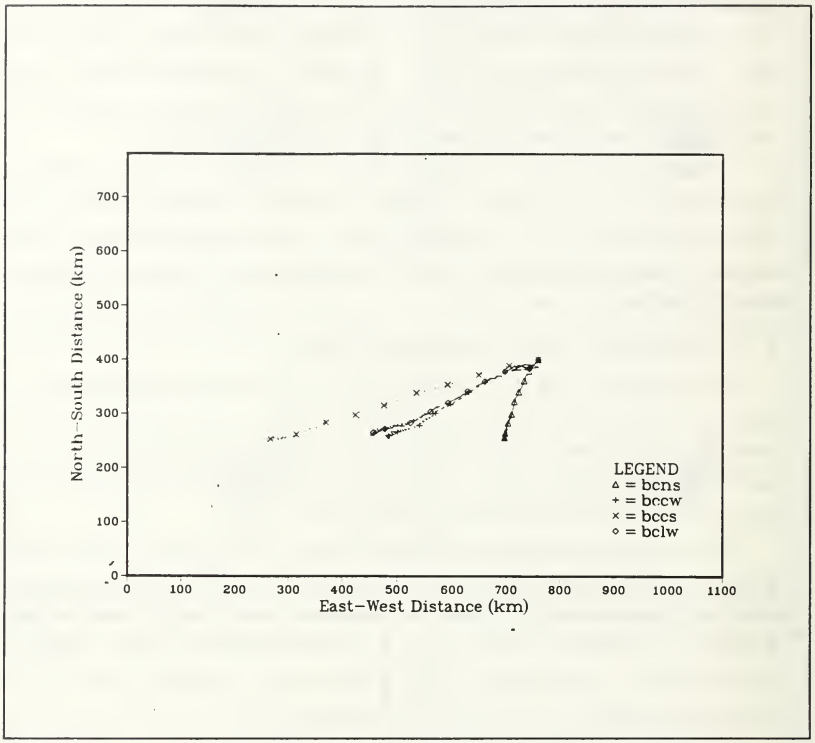

Figure 10. Trajectories for Baroclinic Cases 1-4: The symbols indicate 5 day intervals.

seen. Like the barotropic cases, meridional speed is unaltered by the presence of the shear (3.27 km/day), but the zonal speed (6.21 km/day) is a factor of four greater than in the no background flow case BCNS. As in the barotropic constant shear case (BTCW), the zonal speed in this case is less (5% in this case) than the sum of the previous westward component in BCNS (1.5 km/day) and the constant 5 cm/s (4.32 km/day) background flow.

The dipolar lower layer flow previously seen in experiment BCNS (Figure 9 on page 16) is very comparable in this experiment. Figure 15 on page 23 shows velocity vectors in the lower layer for this case. The cyclonic flow under the eddy is approximately 8

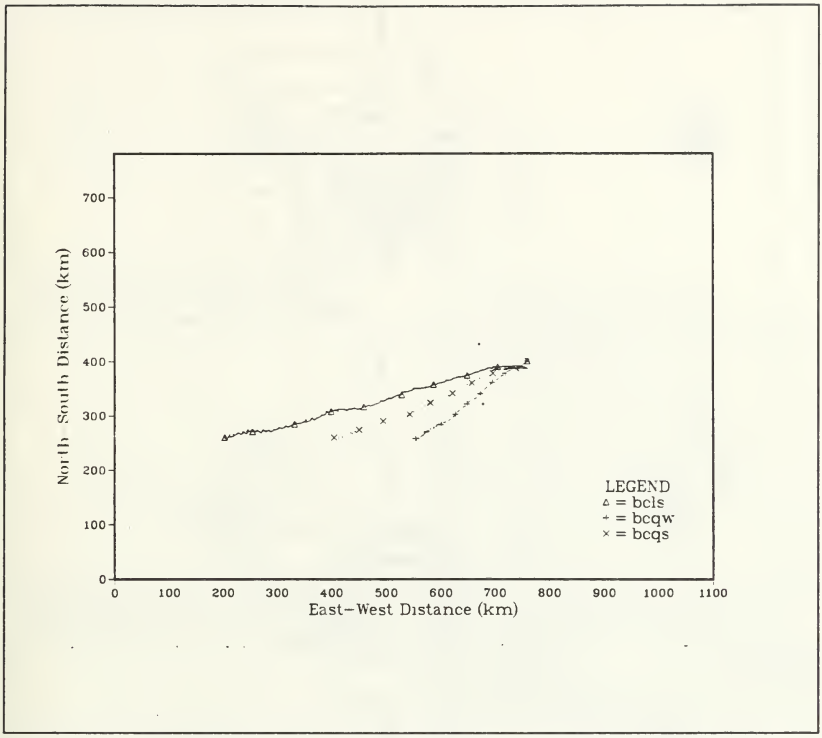

Figure 11. Trajectories for Baroclinic Cases 5-7: The symbols indicate 5 day intervals.

cm/s. The anticyclonic flow is weaker (approximately 2 cm/s). Despite the southward advective effect associated with this lower dipole, this baroclinic anticyclone moves to the south slower than the previous barotropic case (BTCW). The faster dispersion in the barotropic mode explains this difference.

E. BAROTROPIC EDDY, LINEAR SHEAR

Barotropic eddy motion in a linearly sheared background flow (Figure 16 on page 24) is very comparable to that in the constant shear case BTCW. This can be seen by comparing trajectories in Figure 8 on page 15. Meridional speeds are nearly the same with zonal speed slightly higher at 5.5 km/day (vs. 4.0 km/day in the constant shear

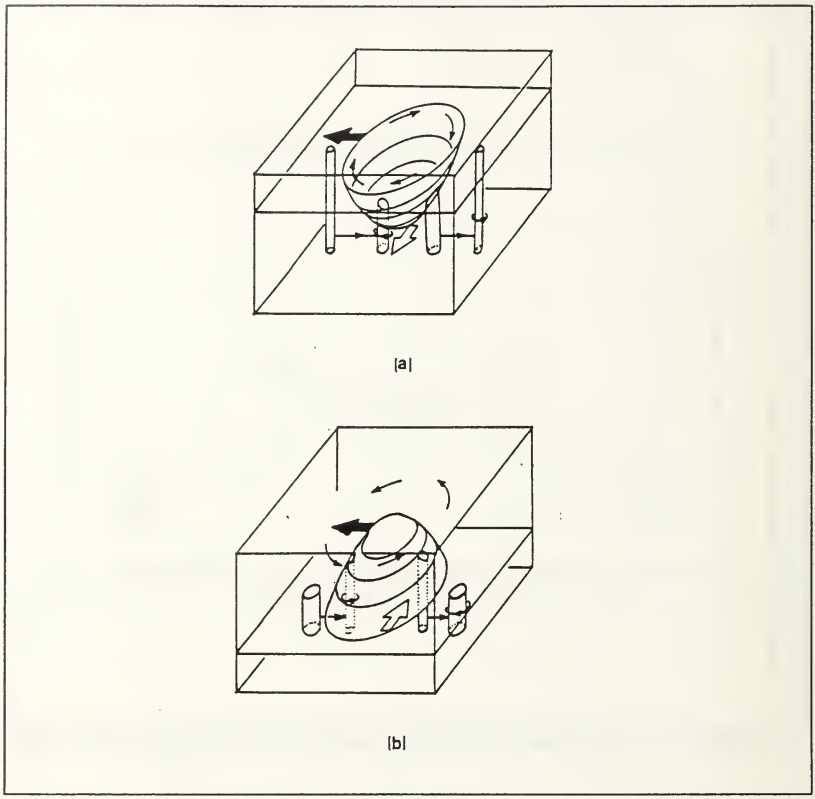

Figure 12. Vortex Stretching of Quiescent Lower Layer Fluids (Cushman-Roisin *et al.*,1989): Impact of the westward migration of an upper-layer eddy on the lower layer and the reaction of the induced lower-layer relative vorticity on the eddy drift: squeezing and stretching under (a) an anticyclone and (b) a cyclone.

case). The higher zonal velocity is associated with the increase in background flow velocities as the eddy moves southward. The divergent region upstream previously seen in the constant shear case is also seen in this experiment as is the trailing cyclonic vortex.

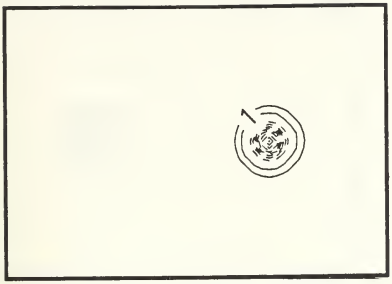

Day 0 Upper Layer Relative Vorticity

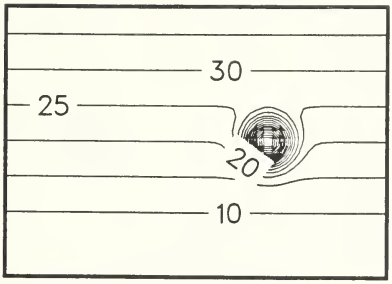

Day 0 Surface Height

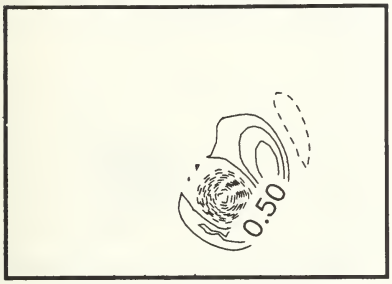

Day 22 Upper Layer Relative Vorticity

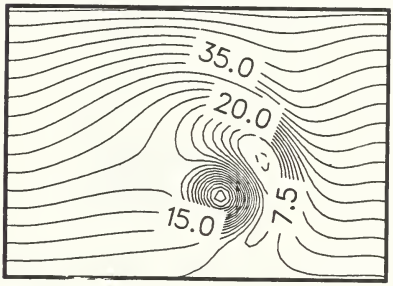

Day 22 Surface Height

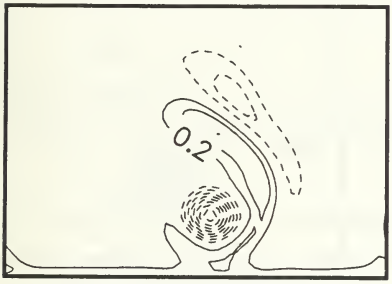

Day 37 Upper Layer Relative Vorticity

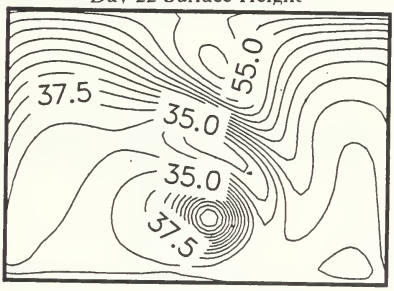

Day 37 Surface Height

Figure 13. Barotropic Eddy, Constant Shear: The left panels are contours of relative vorticity. Positive values are solid, negative values are dashed, and values are $10^{-5}s^{-1}$. The contour intervals are $.5x10^{-5}s^{-1}$ (day 0), $.25x10^{-5}s^{-1}$ (day 22), and $.1x10^{-5}s^{-1}$ (day 37). The right panels are contours of surface height (cm). The contour intervals are 5 cm (day 0), 2.5 cm (day 22), and 2.5 cm (day 37). North is at the top of the figure.

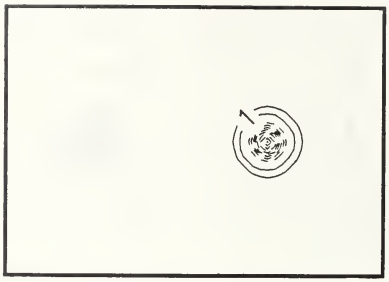

Day 0 Upper Layer Relative Vorticity

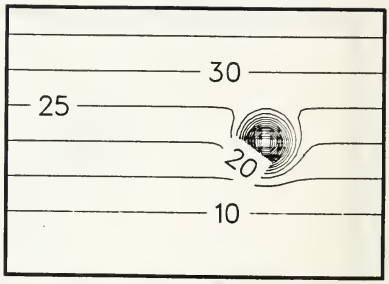

Day 0 Surface Height

Day 22 Upper Layer Relative Vorticity

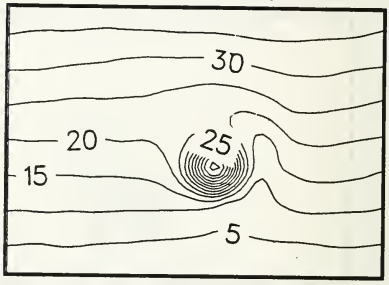

Day 22 Surface Height

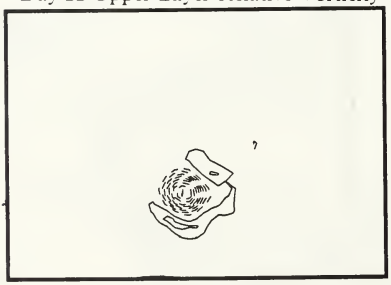

Day 37 Upper Layer Relative Vorticity

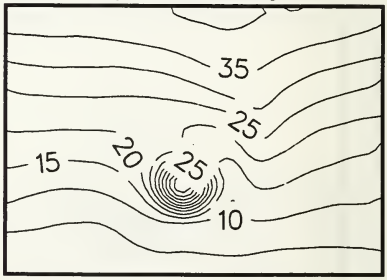

Day 37 Surface Height

Figure 14. Baroclinic Eddy, Constant Shear: The left panels are contours of relative vorticity. Positive values are solid, negative values are dashed, and values are $10^{-5}s^{-1}$. The contour intervals are $.5x10^{-5}s^{-1}$ (day 0), $.25x10^{-5}s^{-1}$ (day 22), and $.1x10^{-5}s^{-1}$ (day 37). The right panels are contours of surface height (cm). The contour intervals are 5 cm (day 0), 5 cm (day 22), and 5 cm (day 37). North is at the top of the figure.

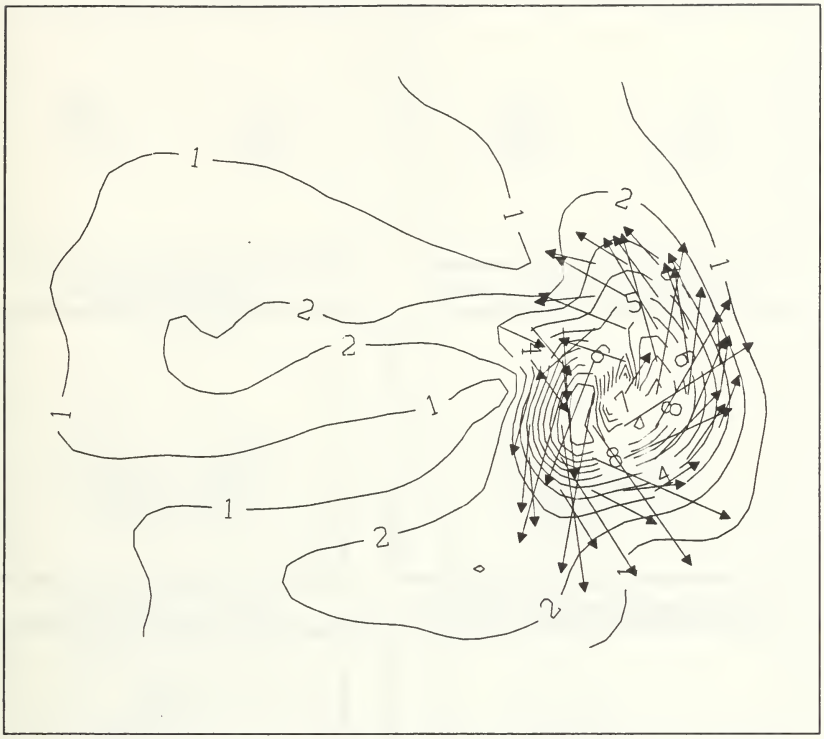

Figure 15. Lower Layer Velocity Vectors and Isotachs for Baroclinic No Shear (day 22): Contours interval is 1 cm/s with arrows indicating magnitude and direction.

F. BAROCLINIC EDDY, LINEAR SHEAR

As in the preceding section, a linear shear (Figure 17 on page 25) only slightly changes meridional baroclinic eddy propagation from the constant (no shear) case. The trajectory (Figure 10 on page 18 and Figure 11 on page 19) for this case is comparable to the no shear case, with zonal speed slightly higher (6.9 vs. 6.2 km/day). These speeds to the west are higher than the corresponding barotropic cases. This is true in the quadratic shear cases also. The reasons for the greater speeds in baroclinic cases are discussed below.

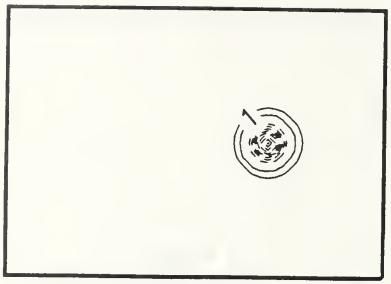

Day 0 Upper Layer Relative Vorticity

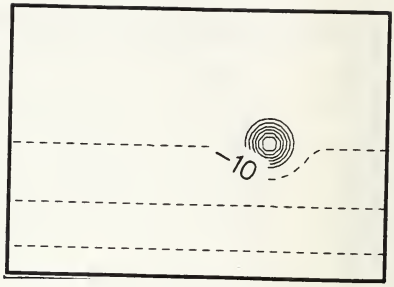

Day 0 Surface Height

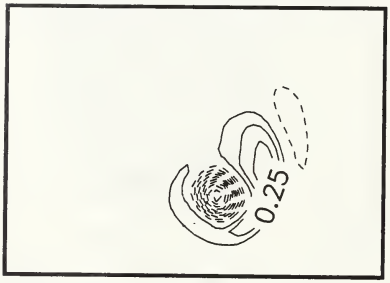

Day 22 Upper Layer Relative Vorticity

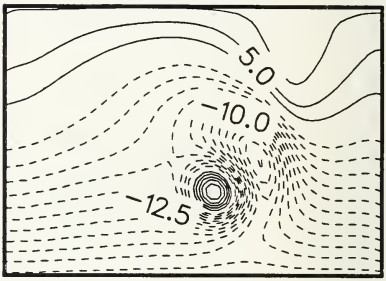

Day 22 Surface Height

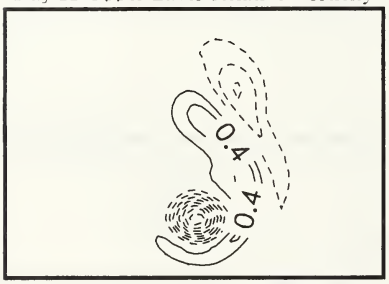

Day 37 Upper Layer Relative Vorticity

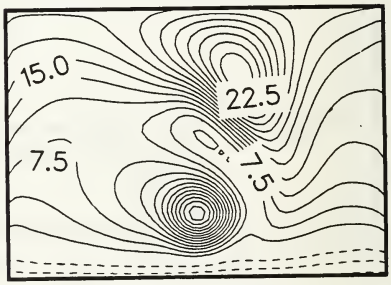

Day 37 Surface Height

Figure 16. Barotropic Eddy, Linear Shear: The left panels are contours of relative vorticity. Positive values are solid, negative values are dashed, and values are $10^{-5}s^{-1}$. The contour intervals are $.5x10^{-5}s^{-1}$ (day 0), $.125x10^{-5}s^{-1}$ (day 22), and $.2x10^{-5}s^{-1}$ (day 37). The right panels are contours of surface height (cm). The contour intervals are 5 cm (day 0), 2.5 cm (day 22), and 2.5 cm (day 37). North is at the top of the figure.

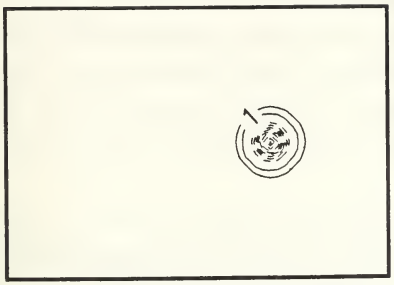

Day 0 Upper Layer Relative Vorticity

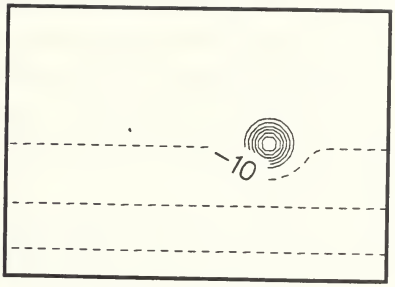

Day 0 Surface Height

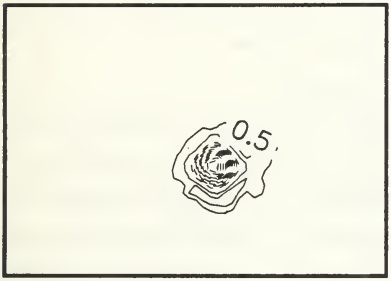

Day 22 Upper Layer Relative Vorticity

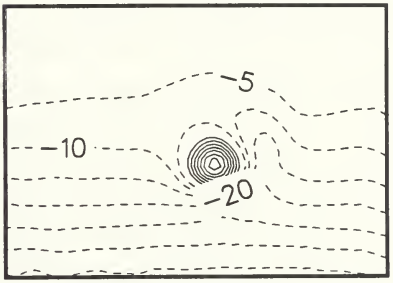

Day 22 Surface Height

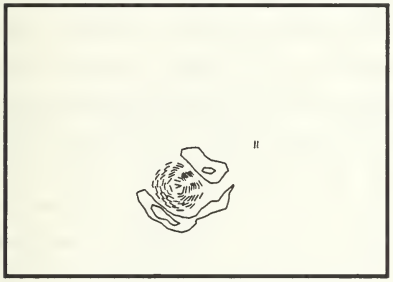

Day 37 Upper Layer Relative Vorticity

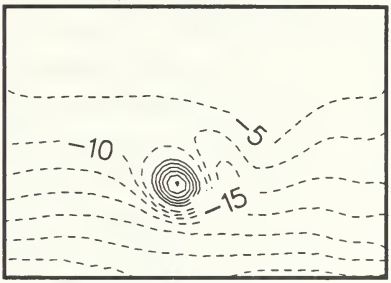

Day 37 Surface Height

Figure 17. **Baroclinic Eddy, Linear Shear:** The left panels are contours of relative vorticity. Positive values are solid, negative values are dashed, and values are $10^{-5}s^{-1}$. The contour intervals are $.5x10^{-5}s^{-1}$ (day 0), $.25x10^{-5}s^{-1}$ (day 22), and $.1x10^{-5}s^{-1}$ (day 37). The right panels are contours of surface height (cm). The contour intervals are 5 cm (day 0), 5 cm (day 22), and 5 cm (day 37). North is at the top of the figure.

G. BAROTROPIC EDDY, QUADRATIC SHEAR

The presence of quadratic shear leads to a slightly higher meridional eddy speed over previous barotropic cases. Zonal speed averages 7.8 km/day (40% greater than the corresponding linear shear case). A comparison of Figure 18 on page 27 with the linear shear case (Figure 16 on page 24) shows only minor differences in the spatial eddy structure.

Figure 19 on page 28 shows velocity vectors and isotachs for this case. A comparison of upper and lower layers indicate that the flow remains barotropic during the experiment. Velocities in the divergent region to the west of the eddy approach zero with time. On day 22, the strongest flow is on the trailing side of the eddy. At this time the eddy center is located at the latitude of 10 cm/s zonal flow.

H. BAROCLINIC EDDY, QUADRATIC SHEAR

As in previous sections, meridional speed (3.2 km/day) is unaltered by the form of the shear and a comparison of Figure 20 on page 29 with the linear shear case (Figure 17 on page 25) shows only minor differences. Zonal speed (8 km/day) is higher than the linear shear case. This is consistent with the stronger flows near the southern boundary (Figure 21 on page 30) in this case relative to the previous shear flows. In contrast to previous cases this speed is also comparable to the barotropic quadratic shear case (BTQW). In previous cases the zonal speed was higher in baroclinic cases.

To examine how background flows modify the eddy motion, the trajectories for baroclinic and barotropic cases were recomputed with the initial background shear flow removed. Figure 22 on page 31 and Figure 23 on page 32 show these trajectories for the barotropic and baroclinic cases respectively. These figures show that a constant shear nearly adds linearly to eddy propagation. The trajectories for linear and quadratic shear cases indicate an eastward component of motion induced in the eddies by background flow. For quadratic shear barotropic case BTQW, for example, the eddy is displaced 120 km in 45 days or an eastward speed of 2.7 km/day relative to the background westward flow. It is interesting to compare the trajectory for the quadratic shear baroclinic case BCQW and the corresponding barotropic case BTQW. While the meridional component of motion in BTQW is higher the zonal components are nearly identical. This is also supported by the mean zonal components for these cases (7.8 amd 8.0 km/day) in Table 2 on page 48 and Table 3 on page 48.

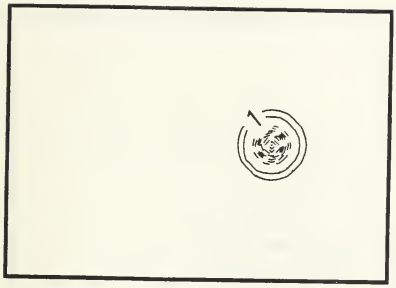

Day 0 Upper Layer Relative Vorticity

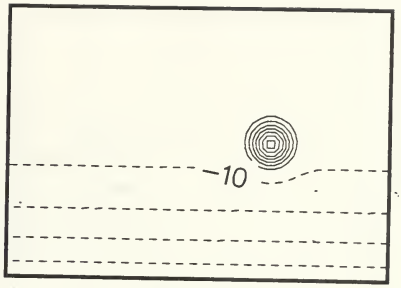

Day 0 Surface Height

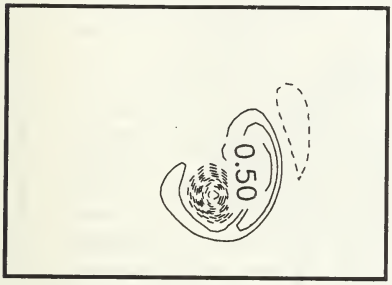

Day 22 Upper Layer Relative Vorticity

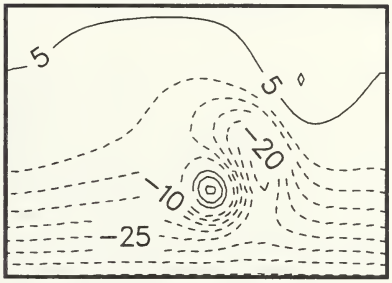

Day 22 Surface Height

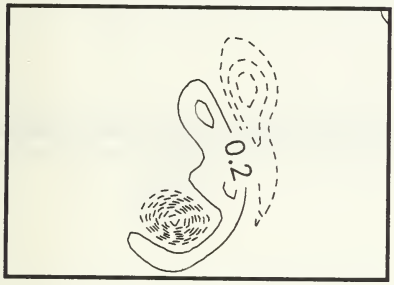

Day 37 Upper Layer Relative Vorticity

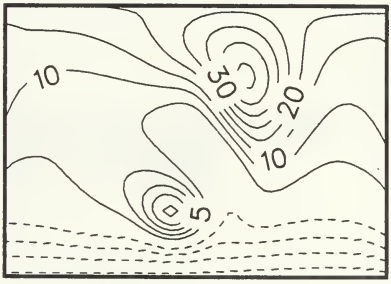

Day 37 Surface Height

Figure 18. Barotropic Eddy, Quadratic Shear: The left panels are contours of relative vorticity. Positive values are solid, negative values are dashed, and values are $10^{-5}s^{-1}$. The contour intervals are $.5x10^{-5}s^{-1}$ (day 0), $.25x10^{-5}s^{-1}$ (day 22), and $.1x10^{-5}s^{-1}$ (day 37). The right panels are contours of surface height (cm). The contour intervals are 5 cm (day 0), 5 cm (day 22), and 5 cm (day 37). North is at the top of the figure.

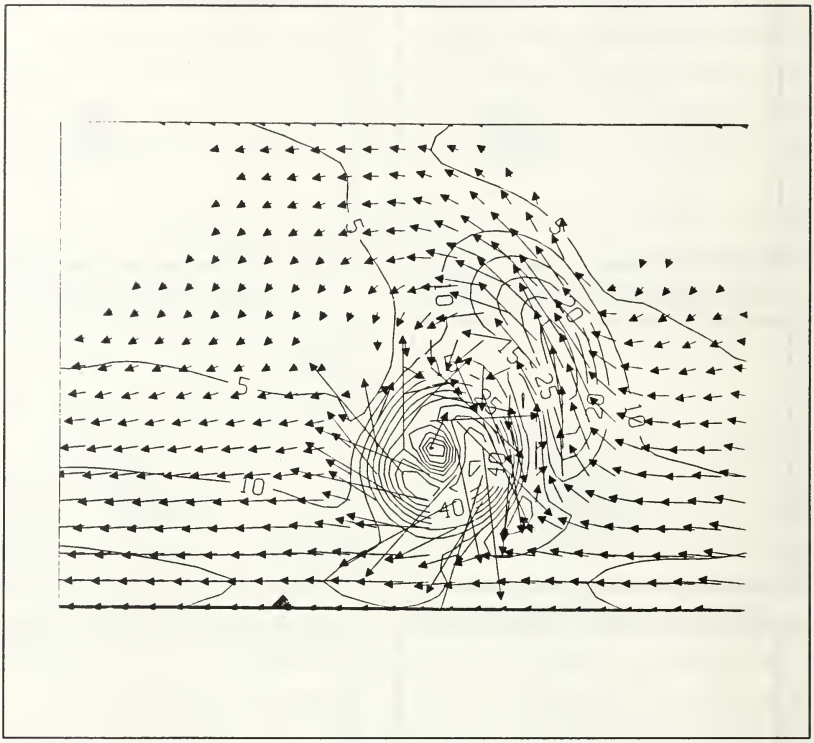

Figure 19. Lower Layer Velocity Vectors and Isotachs for Barotropic Quadratic Shear (day 22): Contour interval is 5 cm/s with arrows indicating magnitude and direction.

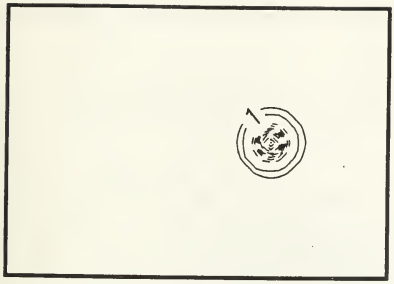

Day 0 Upper Layer Relative Vorticity

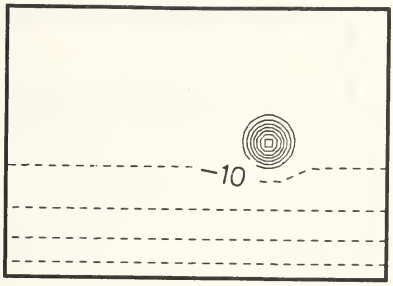

Day 0 Surface Height

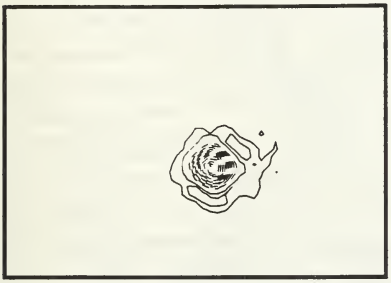

Day 22 Upper Layer Relative Vorticity

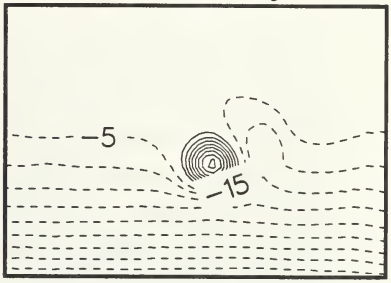

Day 22 Surface Height

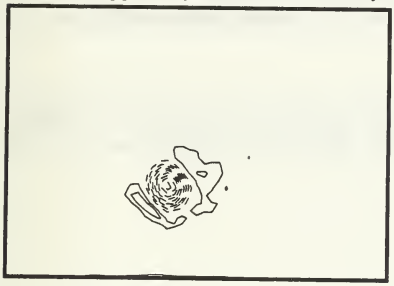

Day 37 Upper Layer Relative Vorticity

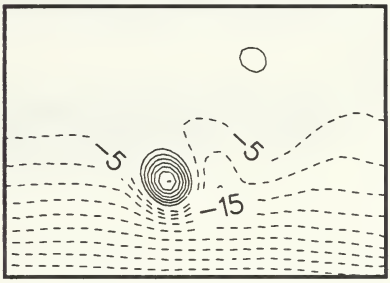

Day 37 Surface Height

Figure 20. **Baroclinic Eddy, Quadratic Shear:** The left panels are contours of relative vorticity. Positive values are solid, negative values are dashed, and values are $10^{-5}s^{-1}$. The contour intervals are $.5x10^{-5}s^{-1}$ (day 0), $.25x10^{-5}s^{-1}$ (day 22), and $.1x10^{-5}s^{-1}$ (day 37). The right panels are contours of surface height (cm). The contour intervals are 5 cm (day 0), 5 cm (day 22), and 5 cm (day 37). North is at the top of the figure.

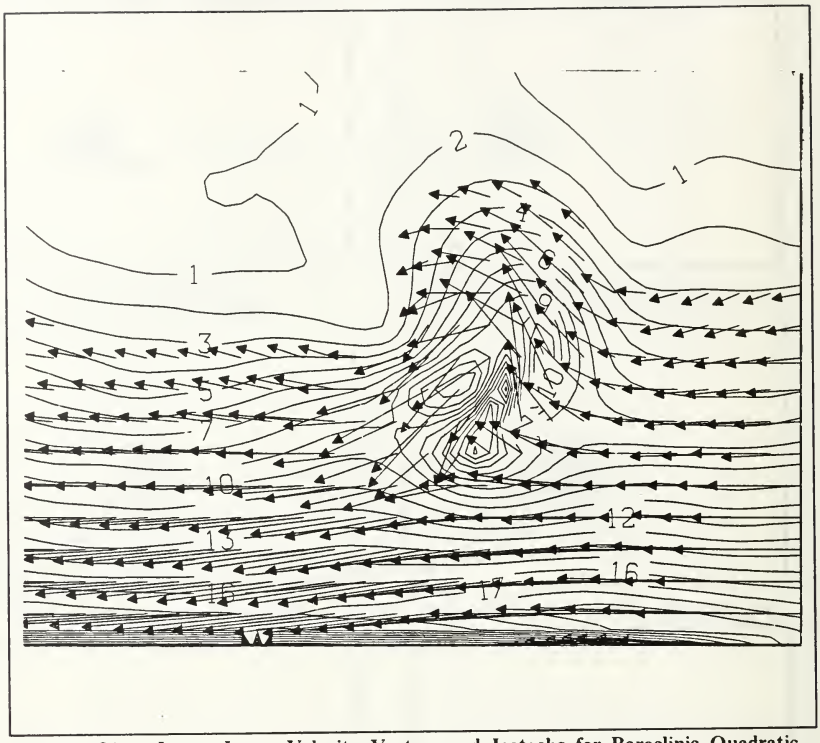

Figure 21. Lower Layer Velocity Vectors and Isotachs for Baroclinic Quadratic Shear (day 22): Contours interval is 1 cm/s with arrows indicating magnitude and direction.

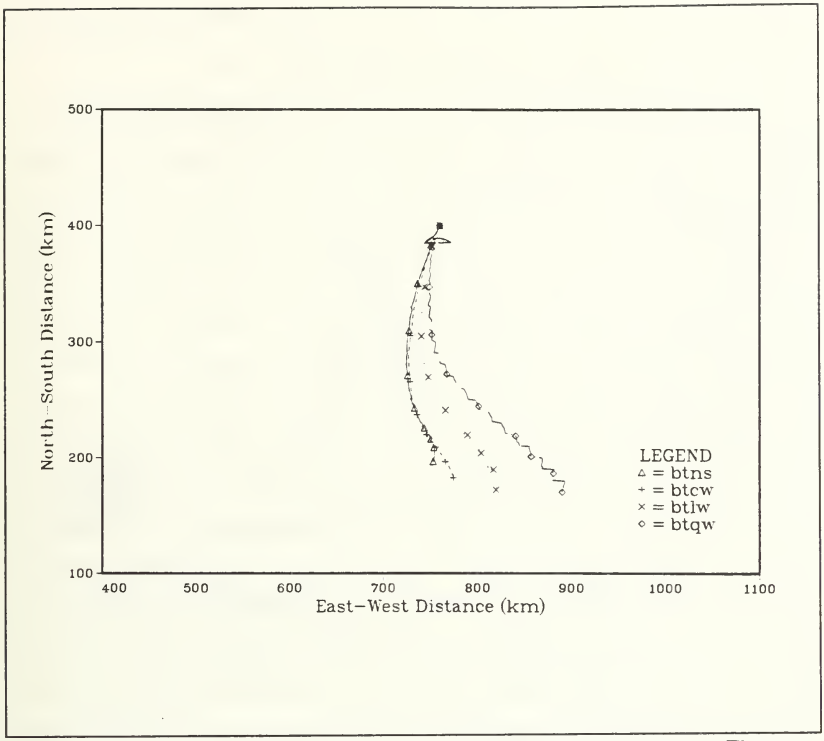

Figure 22. Trajectories for Barotropic Cases Minus Background Shear: The trajectories for barotropic cases were recomputed with the initial background shear flow removed. The symbols indicate 5 day intervals.

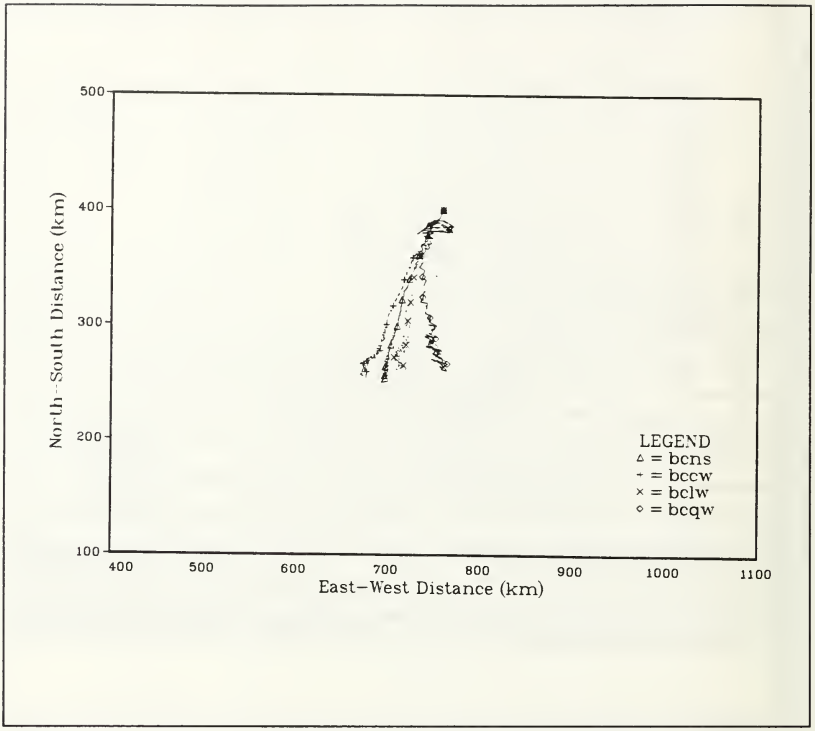

Figure 23. Trajectories for Baroclinic Cases Minus Background Shear: The trajectories for baroclinic cases were recomputed with the initial background shear flow removed. The symbols indicate 5 day intervals.

IV. AZIMUTHAL MODE ANALYSIS

The zonal and meridional average eddy speeds (Table 2 on page 48 and Table 3 on page 48) are consistent with azimuthal distortions in the eddies. In Figure 24 on page 35 and Figure 25 on page 36 the eddies have been decomposed into axisymmetric and asymmetric components. Only the asymmetric portion of the eddy is shown in these figures. The dipolar structure in the majority of the experiments indicates that an azimuthal mode one structure is present. As discussed above, this distortion is caused by Rossby wave dispersion. The β-effect associated with quadratic shear has little effect in offsetting this dispersive behavior. The orientation of the dipolar part provides southward and westward eddy motion in most baroclinic cases. A comparison of the orientation of the dipolar structures in Figure 25 on page 36 indicates that the background shear has little effect in rotating the azimuthal mode one structure. The higher westward eddy speeds for the linear and quadratic shear cases (Table 3 on page 48) thus are related to the higher background flow velocities and not to a rotation of the mode one structure by the shear.

Azimuthal mode one structure is also present in the barotropic cases. Experiments BTNS and BTCW (Figure 24 on page 35) have dipolar corrections to a circular symmetric shape. The orientation of the dipole gives southeastward motion in the case of BTNS and southward for BTCW. The trajectory for BTNS (Figure 8 on page 15) shows eastward motion near the end of the run. In contrast to baroclinic cases (all show azimuthal mode one structure), barotropic cases BTLW and BTQW have higher azimuthal mode structure. The presence of two highs and two lows in Figure 24 on page 35 suggests that these eddies had a more elliptical distribution. The elliptical distributions do not contribute to eddy motion as does azimuthal mode one distribution. A comparison of westward and southward mean speeds (Table 2 on page 48 and Table 3 on page 48) for barotropic and baroclinic eddies reveals that barotropic eddies move faster to the south and slower to the west than baroclinic eddies. This seems inconsistent with the fact the barotropic eddies which propagate further south than baroclinic eddies are advected westward by higher background velocities. The enhanced westward speed for baroclinic eddies appears related to the azimuthal mode orientation which augments the westward β-induced speed. The orientation of the azimuthal mode one structure in the barotropic cases does not give a westward component of motion. In addition, it was

demonstrated above that barotropic eddies in linear or quadratic shear have eastward components of motion relative to the background flow.

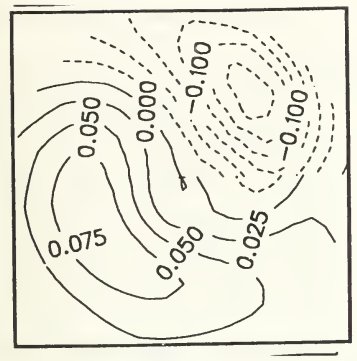

BTNS day 22

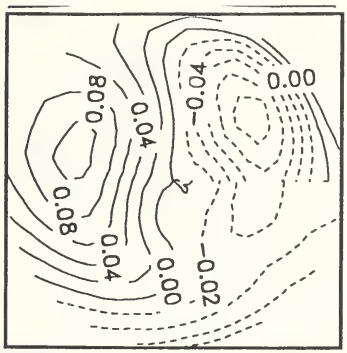

BTCW day 22

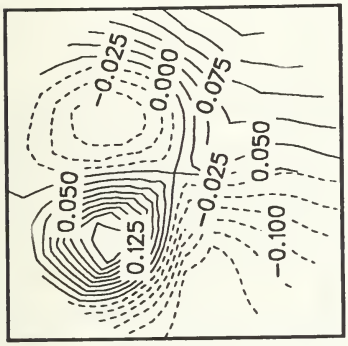

BTLW day 22

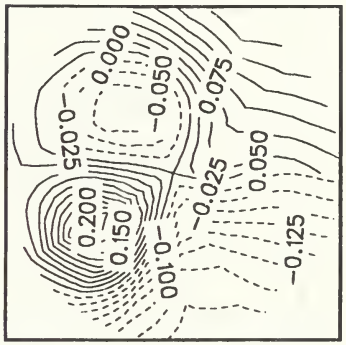

BTQW day 22

Figure 24. Azimuthal Mode Decomposition for Barotropic Cases (day 22): The contour is surface height anomaly after the height associated with the axisymmetric signature of the eddy has been removed. The contour interval equal .025x10^{-1}m for the Barotropic No Shear (BCNS) case, .020x10^{-1}m for the Barotropic Constant Weak (BTCW) case, .025x10^{-1}m for the Barotropic Linear Weak (BTLW) case, and .025x 10^{-1}m for the Barotropic Quadratic Weak (BTQW) case. Weak indicates mid basin flow of .5 m/s. North is at the top of the figure.

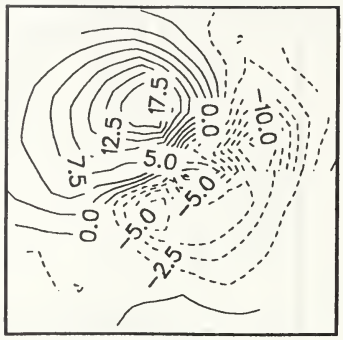

BCNS day 22

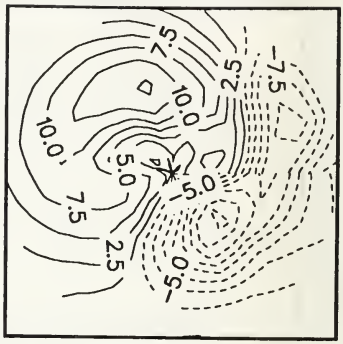

BCCW day 22

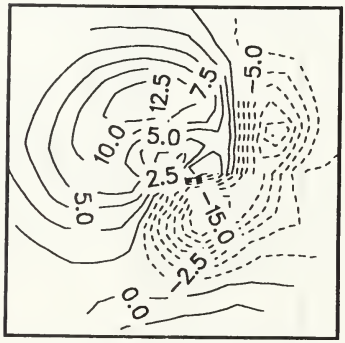

BCLW day 22

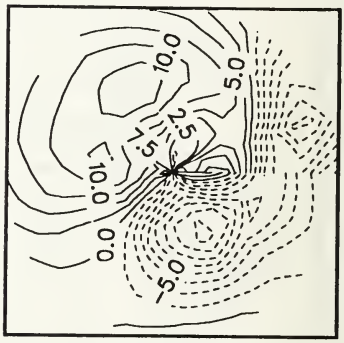

BCQW day 22

Figure 25. Azimuthal Mode Decomposition for Baroclinic Cases (day 22): The contour is interface height anomaly after the height associated with the axisymmetric signature of the interface has been removed. The contour interval equal 2.5×10^{-1}m for the Baroclinic No Shear (BCNS) case, 2.5×10^{-1}m for the Baroclinic Constant Weak (BCCW) case, 2.5×10^{-1}m for the Baroclinic Linear Weak (BCLW) case, and 2.5×10^{-1}m for the Baroclinic Quadratic Weak (BCQW) case. Weak indicates mid basin flow of .5 m/s. North is at the top of the figure.

V. TIME DEPENDENT EDDY MOTION

A. BAROTROPIC CASES

Figure 26 on page 38 shows the zonal eddy speeds as a function of time for all barotropic cases. This figure shows that the eddy speed is time dependent. The eddy speeds plotted in this figure have been averaged into 5 day intervals. In the absence of any background flow (case BTNS), the highest eddy speeds are during the first ten days. An increase in speed during the first 10 days is seen in all cases. This is associated with an adjustment period during which the eddy adjusts from the initial axisymmetric shape to a dispersing eddy. Figure 26 on page 38 also shows that the effect of a constant background flow (case BTCW) is to almost add linearly (within 10%) to eddy speed in the absence of shear. The presence of linear and quadratic shear causes eddy speed to increase with time after day 25 as the eddy propagates into the higher velocity region.

The corresponding meridional motion for all barotropic cases is shown in Figure 27 on page 39. Meridional speeds are also time dependent but little difference exists between the various cases. Eddy adjustment during the first 15 days causes meridional speed to increase during this period. Meridional speed decreases after day 15 associated with rapid barotropic dispersion.

These zonal and meridional speed changes are the result of several factors. Initially, eddy shape adjustments lead to increases in both zonal and meridional speed. Subsequently dispersive weakening of the eddy over time decreases both zonal and meridional speeds. Finally an increase in westward speed is associated with increased zonal background flow (in the linear and quadratic shear cases BTLW and BTQW). For the zonal velocity then, initially dispersive adjustment and decay is important and later, stronger background flow magnitude is important.

B. BAROCLINIC CASES

The time dependent eddy speeds for all baroclinic cases are shown in Figure 28 on page 40 (zonal) and Figure 29 on page 41 (meridional). The baroclinic eddy speeds also show large changes in speed with time. The baroclinic zonal speeds also show a large initial adjustment period during the first 15 days. In contrast to the barotropic cases where eddy speeds increase during the adjustment period, baroclinic cases BCCW and BCLW show decrease in zonal eddy speed initially. Beyond day 15 zonal speeds are relatively constant. The less dispersive baroclinic eddies do not show the slowing seen in

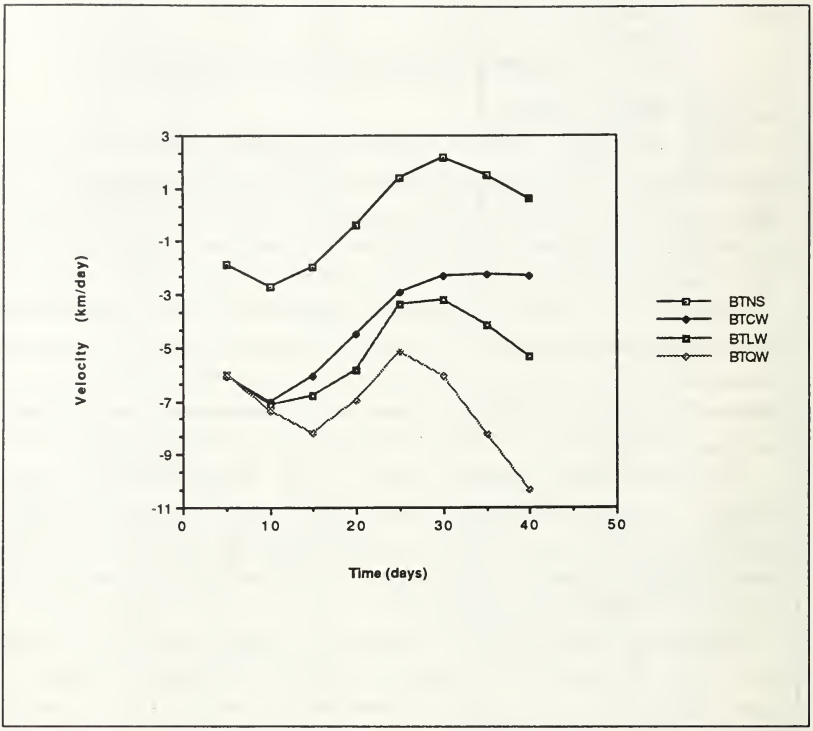

Figure 26. Zonal Time Dependent Speeds for Barotropic Eddies: Mid basin flow is .05 m/s. Positive values represent North for meridional flows and East for zonal flows.

the barotropic cases. There is a slight tendency for baroclinic zonal speeds to increase near the end of the of the 40 day period. All baroclinic meridional speeds decrease to less than several km/day during the first 10 days. This is in contrast to barotropic meridional speeds which increased during the first 20 days. Maximum baroclinic southward speeds reach 4 km/day in contrast to 8 km/day for barotropic cases.

C. TIME AVERAGED ZONAL AND MERIDIONAL EDDY SPEED

Figure 30 on page 42 summarizes average meridional and zonal eddy speeds for barotropic and Figure 31 on page 43 for baroclinic cases. These figures illustrate that

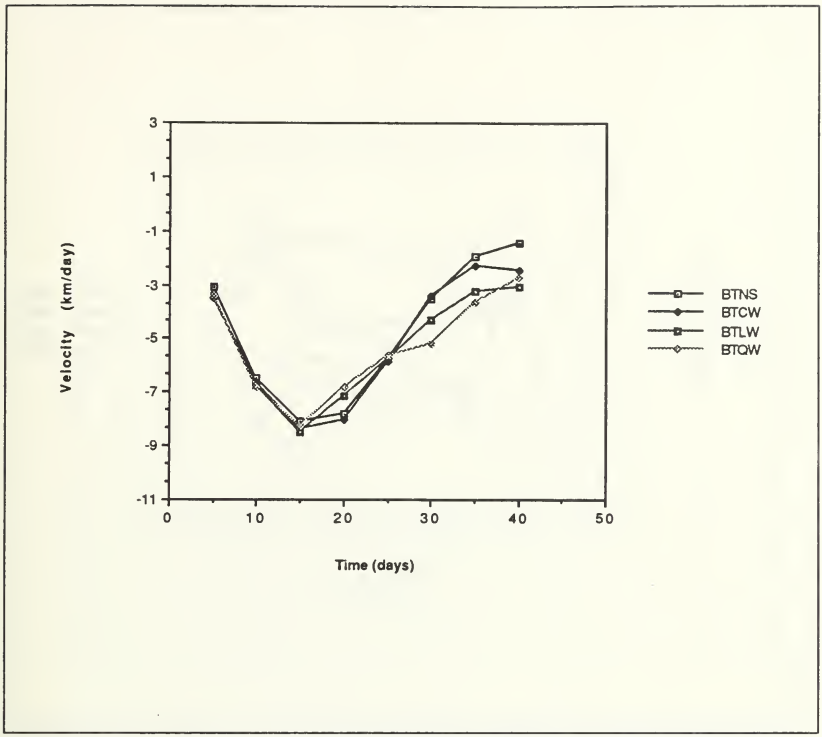

Figure 27. Meridional Time Dependent Speeds for Barotropic Eddies: For .05 m/s mid basin flow

eddy meridional speed is relatively insensitive to the form of background shear, but zonal speed is dependent on the shear profile.

D. COMPARISON WITH OTHER MODEL RESULTS

The model of Cushman-Roisin *et al.* (1989) suggests several eddy propagation tendencies with which these results can be compared. Cushman-Roisin *et al.* (1989) argues that eddy propagation can be influenced by two mechanisms which depend on the eddy vertical structure. For an anticyclone in the upper ocean only, vortex squashing of fluid columns in the lower layer will create anticyclonic vorticity under the leading edge of the eddy. Fluid columns in the lee of the eddy will acquire cyclonic vorticity

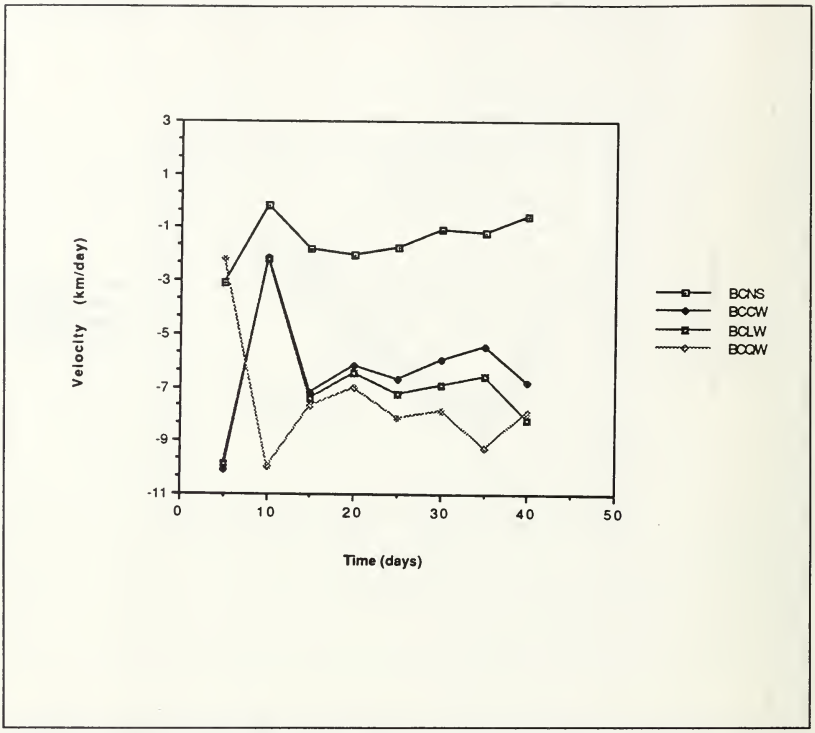

Figure 28. Zonal Time Dependent Speeds for Baroclinic Eddies: For .05 m/s mid basin flow

through vortex stretching. These tendencies were illustrated in Figure 12 on page 20 (from Cushman-Roisin *et al.* 1989). The combined effect is to advect the eddy to the south. For barotropic eddies the fluid columns must move north and south around the eddy in each layer. Fluid columns moving northward acquire anticyclonic vorticity. Fluids columns moving southward around the eddy acquire cyclonic vorticity as the Coriolis parameter decreases. The combined effect of these tendencies is to augment the westward speed of the barotropic anticyclones.

For no background flow, the results of baroclinic experiment BCNS illustrates the Cushman-Roisin *et al.* (1989) baroclinic argument (see Figure 9 on page 16). In the

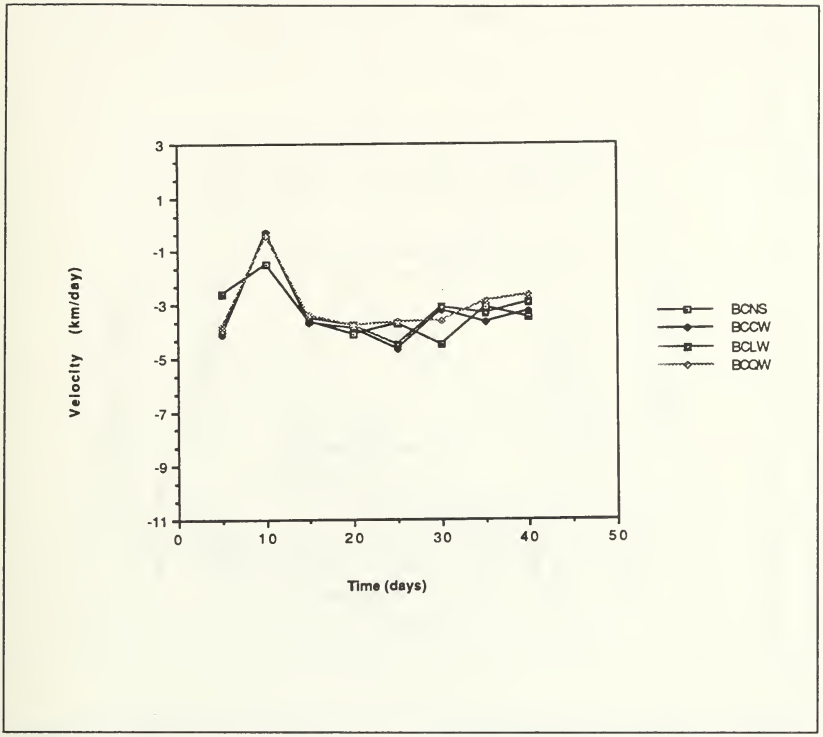

Figure 29. Meridional Time Dependent Speeds for Baroclinic Eddies: For .05 m/s mid basin flow

presence of background flows, these tendencies still apply. Fluid columns in the lower layer should acquire the same vorticity tendencies as they go under the eddy, as the upper layer eddy moves relative to the lower layer mean fluid speed. The Cushman-Roisin *et al* (1989) argument is thus unmodified by a barotropic background flow. The meridional speed for baroclinic cases is nearly independent of background shear flow magnitude and lateral profile.

The Cushman-Roisin *et al.* (1989) barotropic argument can also be modified for background flow. For barotropic background flow with speeds greater than the eddy speed, fluid columns overtaking the eddy must go around the eddy to the north and

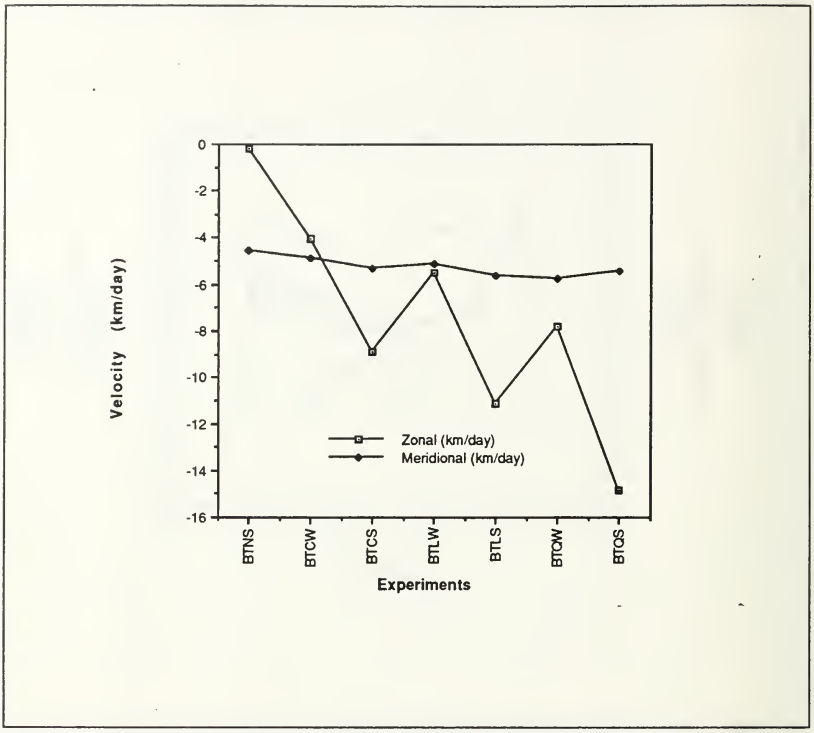

Figure 30. Summary of Time Averaged Meridional and Zonal Speeds for Barotropic Eddies.

south. The northward (southward) displaced columns acquire anticyclonic (cyclonic) vorticity. These effects augment the westward β-induced eddy speed. Figure 6 on page 13 (BTNS) does not show any indication of these vorticity tendencies. Furthermore it was shown in Figure 22 on page 31 that barotropic anticyclones had an eastward component of motion relative to the background flow.

E. COMPARISON WITH OBSERVATIONS

For comparison with the observations of warm core ring propagation by Cornillon *et al.* (1989) and Auer (1987) average speed and direction for barotropic and baroclinic eddy experiments were computed. The averages were based on the experiments with no

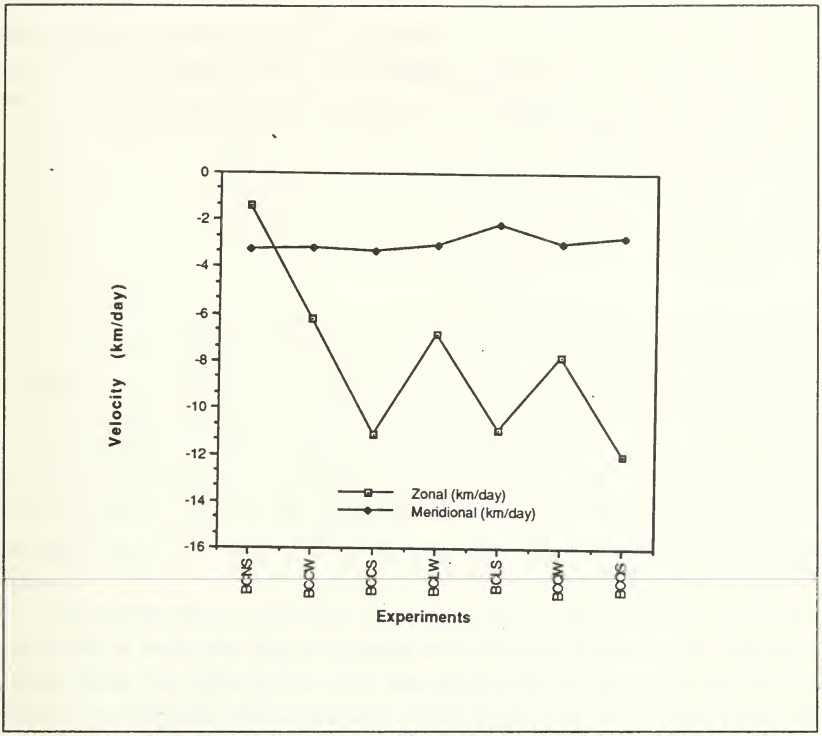

Figure 31. Summary of Time Averaged Meridional and Zonal Speeds for Baroclinic Eddies.

shear or shears with 5 cm/s at mid basin. The resulting speeds are 6.7 km/day at 230° from north for barotropic eddies and 6.4 km/day at 241° for baroclinic eddies. Based on observations of 66 warm core rings, Auer (1987) found a mean speed of 2.4 km/day at 256°.

Eddy speeds in experiments here are considerably higher than the observations suggest. Higher speeds in these experiments suggest that background in the model flow exceed those to the north of the Gulf Stream.

Results here do not explain the northward component of motion for warm core rings east of 70° W observed by Cornillon *et al.* (1989). Their study, based on 11 warm core

rings, gives a mean 8.5 km/day at 282° from north illustrating northward motion of rings relative to the slope water. None of the shear flows chosen here provide this tendency. Observations of warm core ring velocities from other investigators are shown in Appendix C. This table illustrates that estimates of warm core ring speeds vary widely ranging 5 to 7 km/day.

VI. SUMMARY

The effect of background shear flows on ocean eddy motion has been considered using a two-layer numerical model. The results indicate that eddy meridional motion is not dependent on the magnitude or form of the background shear profile. This is true for barotropic and baroclinic experiments. Initially barotropic eddies have higher meridional speeds than baroclinic eddies due to faster Rossby wave dispersion in barotropic eddies.

Eddy zonal speed depends on the initial vertical velocity profile of the eddy. Barotropic eddies propagate slower to the west in all cases than do baroclinic eddies despite the fact that barotropic eddies propagate further into the high velocity regions of the background flow. The higher baroclinic speeds are associated with azimuthal mode one distortions. These distortions have an orientation which advects the baroclinic eddy southwestward. The β induced westward motion is thus augmented by this azimuthal mode one distortion. Barotropic eddies can have azimuthal mode one distortions but the orientation of these does not give westward motion in these experiments.

None of the results in this thesis appear to explain the observations by Cornillon *et al.* (1989) of warm core rings propagating northwestward relative to the background Slope Water. The eddies in that study were presumably not interacting with the Gulf Stream or continental slope topography. The close proximity of the Gulf Stream with the continental slope however makes these interactions likely. From this standpoint, the results of Stern and Flierl (1987) may be applicable. Their results suggest northward motion for anticyclones interacting with the cyclonic shear on the north side of the Gulf Stream. They showed that these interactions could induce northward eddy motion for eddies as far away from the Gulf Stream as several Rossby radii (100-150 km).

APPENDIX A. SYMBOLS AND NOTATION

B_h	biharmonic lateral friction coefficient = $.2x10^{11}$	
f_0	Coriolis parameter for mean latitude 40°N	
g	Gravitational acceleration	
g'	Reduced gravitational acceleration	$= g\frac{\rho_2 - \rho_1}{\rho_1} = .02$
h_i	Instantaneous upper (i = 1) and lower (i = 2) layer thickness	
H_i	Upper (i = 1) and lower (i = 2) layer mean thickness	
L_e	e-folding scale for the eddy	= 40 km
L	North-south domain length	= 780 km
p_1	Pressure in the upper layer	$= g(h_1 + h_2 + d)$
p_2	Pressure in the lower layer	$= p_1 - g'h_1$
R_d	First internal Rossby radius of deformation	$= \sqrt{\frac{g' H_1 H_2}{H_1 + H_2}} = 40$ km
R_0	Rossby number	$= \frac{V_{max}}{fL}$
u_i, v_i	Velocities in the x and y directions	
U_i, V_i	Transport in the x and y directions	

x,y	Cartesian coordinates directed N and W respectively	
γ	nondimensional eddy size	
$\Delta x, \Delta y$	Grid spatial resolution	($2\Delta x$ = 20 km)
Δt	Model time step	4200 sec
ρ_i	Density in i^{th} layer	
∇	Gradient operator	$= \frac{\partial}{\partial x} + \frac{\partial}{\partial y}$
∇^4	biharmonic operator	$= \frac{\partial^4}{\partial x^4} + \frac{\partial^4}{\partial y^4}$

APPENDIX B. TIME-AVERAGED EDDY TRANSLATIONAL SPEEDS

Table 2. INITIALLY BAROTROPIC ANTICYCLONES

Exp	Zonal Speed (km/day)	Meridional Speed (km/day)	Average Speed (km/day)	Lateral Shear (m/sec)
BTNS	-0.17	-4.57	5.53	No Shear
BTCW	-4.02	-4.89	7.80	Constant (.054)
BTCS	-8.89	-5.31	12.12	Constant (.108)
BTLW	-5.50	-5.12	9.11	Linear (.054)
BTLS	-11.12	-5.66	14.67	Linear (.108)
BTQW	-7.80	-5.77	10.88	Quadratic (.054)
BTQS	-14.83	-5.43	18.15	Quadratic (.108)

Table 3. INITIALLY BAROCLINIC ANTICYCLONES

Exp	Zonal Speed (km/day)	Meridional Speed (km/day)	Average Speed (km/day)	Lateral Shear (m/sec)
BCNS	-1.51	-3.38	7.17	No Shear
BCCW	-6.21	-3.27	12.54	Constant (.054)
BCCS	-11.26	-3.33	17.97	Constant (.108)
BCLW	-6.94	-3.19	13.32	Linear (.054)
BCLS	-12.55	-3.13	18.84	Linear (.108)
BCQW	-8.00	-3.15	13.93	Quadratic (.054)
BCQS	-14.69	-3.18	19.18	Quadratic (.108)

APPENDIX C. WARM CORE RING SPEEDS

Table 4. OBSERVED WARM CORE RING SPEEDS

Investigator	Observed Speed (km/day)	Mean Speed (km/day)	Number of Rings
Cheney (1976)	-	5.0	1
Bisagni (1976)	6.1 - 8.3	7.0	13
Lai and Richardson (1977)	3 - 7	-	20
Halliwell and Mooers (1979)	1.7 - 13.0	5.2	14
Brown *et al.* (1886)	1.4 - 11.9	5.6	87
Auer (1987)	-	2.4	66
Cornillon *et al.* (1989)	-	8.5	11

REFERENCES

Adem, J., 1956: A series solution for the barotropic vorticity equation and its application in the study of atmospheric vortices. *Tellus*, **8**, 364-372.

Auer, S.J., 1987: Five-year climatological survey of the Gulf Stream system and its associated rings. *J. Geophys. Res.*, **92**, 11709-11726.

Bisagni, J.J., 1976: Passage of anticyclonic Gulf Stream eddies through deep water dumpsite 106, during 1974 and 1975. NOAA Dumpsite Evaluation Report 76-1, Department of Commerce, 39pp.

Brown, O.B., C.P. Cornillon, S.R. Emmerson, and H.M. Carle, 1986: Gulf Stream warm rings: A statistical study of their behavior. *Deepsea Res.*, **33**, 1459-1473.

Camerlengo, A., and J.J. O'Brien, 1980: Open boundary conditions in rotating fluids. *J. Comp. Phys.*, **35**, 12-35, 1980.

Cheney, R.E., and P.L. Richardson, 1976: Observed decay of a cyclonic Gulf Stream ring. *Deep Sea Res.*, **23**, 143-155.

Cornillon, P., R.Weyer, and G.R.Flierl, 1989: Translational velocity of warm core ring relative to the Slope Water. *J. Phys. Oceanogr.*, 1317-1332.

Cushman-Roisin, B., E. P. Chassignet, and B. Tang, 1989: Westward Motion of Mesoscale Eddies. *J. Phys. Oceanogr.*, **20**, 758-768.

Halliwell, G.R., and C.N.K. Mooers, 1979: The space-time structure and variability of the shelf water-slope water front and Gulf Stream temperature fronts and associated warm core rings. *J. Geophys. Res.*, **84**, 7707-7725.

Hurlburt, H.E., and J.D. Thompson, 1980: A numerical study of Loop Current intrusions and eddy shedding. *J. Phys. Oceanogr.*, **10**, 1611-1651.

Ikeda, M. and J. Apel, 1981: Mesoscale eddies detached from spatially growing meanders in an eastward flowing oceanic jet using a two-layer quasi geostrophic model. *J. Phys. Oceanogr.*, **11**, 1638-1661.

Ingersoll, A.P., and P.G. Cuong, 1981: Numerical model of longlived Jovian vortices. *J. Atmos. Sci.*, **38**, 2067-2076.

Lai, D.V. and P.L. Richardson, 1977: Distribution and movement of Gulf Stream rings. *J. Phys. Oceanogr.*, **7**, 670-683.

Matsuura, T., and T. Yamagata, 1982: On the evolution of nonlinear planetary eddies larger than the Rossby radius of deformation. *J. Phys. Oceanogr.*, **12**, 440-456.

McWilliams, J.C. and G.R. Flierl, 1979: On the evolution of isolated nonlinear vortices. *J. Phys. Oceanogr.*, **9**, 1155-1182.

Mied, R.P. and G.J. Lindemann, 1979: The propagation and evolution of cyclonic Gulf Stream rings. *J. Phys. Oceanogr.*, **9,** 1183-1206.

Nof, D. and C. Shi, 1989: Interaction of Cold and Warm core rings with environmental shear. *J. Phys. Oceanogr.*, **19,** 890-900.

Rossby, C.G., 1948: On the displacement and intensity change of atmospheric vortices. *J. Mar. Res.*, **7,** 175-186.

Smith, D.C.,IV and A.A. Bird, 1989: Factors influencing asymmetry and self advection in ocean eddies. The 20th Annual Symposium on Ocean Hydrodynamics. Elsevier Oceanography Series, Nihoul, ed., 211-225.

Smith, D.C.,IV and J.J. O'Brien, 1983: The interaction of a two layer isolated mesoscale eddy with bottom topography, *J. Phys. Oceanogr.*, **13,** 1681-1697.

Smith, D.C.,IV and R.O. Reid, 1982: A numerical study of non-frictional decay of mesoscale eddies. *J. Phys. Oceanogr.*, **12,** 244-255.

Stern, M.E. and G.R. Flierl, 1987: On the interaction of a vortex with a shear flow, *J. Geophys. Res.*, **92,** 10733-10744.

INITIAL DISTRIBUTION LIST

		No. Copies
1.	Defense Technical Information Center Cameron Station Alexandria, VA 22304-6145	2
2.	Library, Code 52 Naval Postgraduate School Monterey, CA 93943-5002	2
3.	Chairman (Code OC/Co) Department of Oceanography Naval Postgraduate School Monterey, CA 93943-5000	1
4.	Chairman (Code MR/Hy) Department of Meteorology Naval Postgraduate School Monterey. CA 93943-5000	1
5.	Professor David C. Smith IV, (Code OC/Si) Department of Oceanography Naval Postgraduate School Monterey, CA 93943-5000	1
6.	Arlene Bird (Code OC/Bi) Department of Oceanography Naval Postgraduate School Monterey, CA 93943-5000	1
7.	Chief, Career Development Division Office of NOAA Corps Operations NOAA (CPC2) Rockville, MD 20852	1
8.	Chief of Naval Research 800 North Quincy Street Arlington, VA 22217	1
9.	Director Naval Oceanography Division Naval Observatory 34th and Massachusetts Avenue NW Washington, DC 20390-5000	1
10.	Commander Naval Oceanography Command Stennis Space Center MS 39529-5000	1

11. Commanding Officer 1
Fleet Numerical Oceanography Center
Monterey, CA 93943-5005

12. Professor Wendall A. Nuss (Code MR/Nu) 1
Department of Meteorology
Naval Postgraduate School
Monterey, CA 93943-5000

13. Professor R. T. Williams (Code MR/Wu) 1
Department of Meteorology
Naval Postgraduate School
Monterey. CA 93943-5000